

NAG5-1653

*Final Report to  
The National Aeronautics and Space Administration  
on studies of*

JN-47-012

13751

511

# Water and Climate

*Principal Investigator: David A. Randall*

*Department of Atmospheric Science  
Colorado State University  
Fort Collins, Colorado 80523*

June 1994

(NASA-CR-196100) WATER AND CLIMATE  
Final Report (Colorado State  
univ.) 51 p

N95-10093

Unclass

G3/47 0013751



## **I. Summary of Accomplishments**

This research project involved the investigation the vertical profiles of temperature and moisture in convective regimes, using moist available energy as a guide. The results have been used to develop an improved cumulus parameterization.

From a human perspective, kinetic energy is the most important energy form of the atmosphere. All weather systems owe their existence directly to the kinetic energy that they possess. Whether a weather system is intensifying or weakening depends on if it is gaining or losing kinetic energy. Therefore, the source or sink of kinetic energy is a matter of importance. When the source of kinetic energy is huge and increasing, we can predict that the associated weather system will develop and persist and what intensity it will reach; on the other hand, when the source of kinetic energy is limited and decreasing, we can conclude that the associated weather system will weaken. Under adiabatic and frictionless conditions the total energy of the atmosphere, which is the sum of its kinetic energy, potential energy and internal energy, would remain constant. In such a case, the only sources or sinks for the kinetic energy of the whole atmosphere would then be potential energy and internal energy.

Generally speaking, however, the motion of the atmosphere is neither adiabatic nor frictionless. The most important nonadiabatic process which directly alters the atmospheric kinetic energy is friction, which ordinarily generates internal energy or does work on the ocean to increase the ocean's kinetic energy, while destroying the kinetic energy of the atmosphere. Since the intensification of a weather system is often directly related to the production of its kinetic energy, the loss of kinetic energy due to friction is not so important compared to the kinetic energy production. This is especially true when we deal with a short time scale, for instance, several hours or days. As a result, we can sometimes usefully consider a frictionless atmosphere. The other nonadiabatic processes do not alter the kinetic energy of the atmosphere directly, but only alter the internal energy. Therefore, the effects of these processes on the atmosphere can be reflected through the change of internal energy. Hence, after assuming frictionless motion, the



only sources for the kinetic energy of the whole atmosphere are its potential energy and internal energy.

For a column of air standing from the surface to the top of the atmosphere, the vertically integrated total potential energy, defined as the sum of potential energy and internal energy, equals the vertically integrated enthalpy. For the whole atmosphere, the sum of the enthalpy and kinetic energy is conserved under adiabatic and frictionless conditions. This means that the only source of kinetic energy is the enthalpy of the atmosphere. When the enthalpy of the atmosphere decreases adiabatically, the kinetic energy increases.

As discussed by Lorenz (1955), however, the enthalpy (or the total potential energy) is not a good measure of the amount of energy available for conversion into kinetic energy under adiabatic and frictionless flow, since in the atmosphere, not all of the enthalpy can be converted into kinetic energy. A simple example was given by Lorenz (1955) to illustrate this point. Consider first an atmosphere whose density stratification is everywhere horizontal. In this case, although total enthalpy is plentiful, none at all is available for conversion into kinetic energy. Next, suppose that the horizontally stratified atmosphere becomes heated in a restricted region. This heating adds the total enthalpy of the atmosphere, and also disturbs the stratification, thus creating horizontal pressure forces which may convert enthalpy into kinetic energy. On the other hand, suppose that the horizontally stratified atmosphere becomes cooled rather than heated. The cooling removes enthalpy from the system, but it still disturbs the stratification, thus again creating horizontal pressure forces which may convert enthalpy into kinetic energy. Evidently cooling is sometimes as effective as warming in producing kinetic energy, and the total enthalpy itself is not a good measure of how much enthalpy is available for conversion into kinetic energy. It seems that only that portion of enthalpy which can be increased or decreased by the atmospheric motion can be used as the source of kinetic energy.

We therefore desire a quantity which only measures this portion of total potential energy which is available for conversion into kinetic energy under adiabatic and frictionless flow.



According to Lorenz (1955), a quantity of this sort was first discussed by Margules (1903) in his famous paper concerning the energy of storms. Margules considered a closed system possessing a certain distribution of mass. Under adiabatic flow, the mass may be redistributed, with an accompanying change in total potential energy, and an equal and opposite change in kinetic energy. If the stratification becomes horizontal and statically stable, the total potential energy reaches its minimum possible value, and the kinetic energy thus reaches its maximum. This maximum gain of kinetic energy equals the maximum amount of total potential energy available for conversion into kinetic energy under any adiabatic redistribution of mass, and therefore was called “available kinetic energy” by Margules.

The concept of “available potential energy,” which is similar to the “available kinetic energy” defined by Margules, was introduced by Lorenz (1955) in considering the general circulation of the atmosphere. The available potential energy (APE) of the whole atmosphere is defined as the difference between the total potential energy of the whole atmosphere and the minimum total potential energy that the whole atmosphere would have if the mass were redistributed adiabatically to yield a horizontally uniform and vertically stable stratification.

As demonstrated by Lorenz (1955), the APE, so defined, possesses the following important properties:

- (1) Under adiabatic flow, the sum of the available potential energy and the kinetic energy is conserved. The APE is the only source of kinetic energy, but it is not the only sink.
- (2) The available potential energy is completely determined by the distribution of mass.
- (3) The available potential energy is zero if the stratification is horizontally and statically stable. Also, the APE is positive if the stratification is not both horizontally and statically stable.

The “reference state” is defined as the state in which the atmosphere has the minimum total enthalpy that could be reached by rearranging the mass under reversible adiabatic processes.



Then, for any given state of the atmosphere, the APE is defined as the enthalpy difference between the given state and its reference state.

Lorenz (1955) discussed in detail the APE of the whole atmosphere. Although solar radiation is the ultimate source of the atmospheric energy, the atmosphere does not obtain its energy only through solar radiation. It also obtains energy from terrestrial radiation, latent and sensible heat fluxes from the Earth's surface. The globally and annually averaged energy balance (e.g., Peixoto and Oort, 1992; the specific numbers below are from Ramanathan, 1987) shows that the largest energy source for the atmosphere is the latent heat flux from the surface, mainly the ocean surface, with  $90 \text{ W m}^{-2}$ . The atmospheric absorptions of solar and solid earth radiation, 68 and  $63 \text{ W m}^{-2}$  respectively, are smaller, compared to the latent heat flux from the ocean surface; while the surface sensible heat flux is the smallest atmospheric energy source, with  $16 \text{ W m}^{-2}$ .

An essential feature of the solar radiation as received by the Earth is that it is horizontally non-uniform. And of course, the Earth's surface is also non-uniform. Because of these non-uniformities, the latent and sensible heat fluxes from the surface into the atmosphere and the heating and cooling of the atmosphere due to solar and terrestrial radiation are larger in the tropics than in the higher-latitude regions. As a result, a temperature contrast between the equator and the poles is produced. The unbalanced pressure forces demanded by the temperature contrast produce a circulation to transport energy from the region of net energy gain to the region of net energy loss. Thus, most of the APE in the atmosphere is associated with the horizontal temperature contrast which is generated by the horizontally non-uniform energy supply.

As discussed above, the APE is that portion of the total potential energy which can be converted into kinetic energy. There is no assurance that all of the APE will be converted into kinetic energy, however. How much of the APE will be converted varies from case to case. For the whole atmosphere, Lorenz (1955) estimated that the amount of kinetic energy is only about 10% of the amount of APE. Evidently, if kinetic energy is not fully maximized, it is not because a supply of APE is lacking, but because there are not dynamically realizable circulations that can extract all of



the APE.

In Lorenz's (1955) study, however, the role of moisture in the APE was not discussed specifically. Since most of the Earth's surface is covered by the oceans, the evaporation of sea water leads to a large amount of water (mostly in the vapor state) in the atmosphere. Many of the more spectacular weather events, from tropical hurricanes to polar blizzards, owe their existence to the latent energy of condensation and the fusion of water in the atmosphere. Therefore, it is more reasonable to deal with a moist atmosphere than a dry atmosphere in consideration of the APE.

The greatest difficulty in dealing with the APE of moist atmosphere is to include the effects of the latent heat of condensation and fusion of water vapor in the definition of the APE. In the real atmosphere, when condensation happens, latent heat is released, and some of the condensate will drop out as precipitation. This precipitation process is, of course, nonadiabatic, whereas the APE is defined in terms of adiabatic processes. If we assume, however, that all the condensate accompanies the air in which it condenses, the process is still adiabatic. In such a case, the sum of enthalpy and kinetic energy is still conserved, and therefore, the concept of APE is still applicable. Based on this idea, Lorenz (1978,1979) extended the concept of APE to the moist atmosphere. With the effects of water condensation included in the definition of the enthalpy, the APE was called the moist available energy (MAE) by Lorenz (1978,1979), in contrast with the "dry available energy" (DAE) which does not include moisture effects. Lorenz (1978,1979) showed, through both graphical and numerical methods, that the MAE is always larger than the DAE, due to the condensation of some water vapor and the much smaller enthalpy of condensed water compared to water vapor. This shows that the latent heat of water vapor represents an additional source of atmospheric kinetic energy.

When the mass of the whole atmosphere is rearranged adiabatically from the given state to the reference state, the rearrangement is both horizontal and vertical. The horizontal rearrangement is needed to eliminate the horizontal pressure differences and temperature contrasts, while the vertical rearrangement is needed to maximize the static stability. The horizontal rearrange-



ment of mass drives planetary and synoptic circulations whose time scale is days; whereas the vertical rearrangement mostly drives convection whose time scale is several hours. Therefore, the “horizontal part” of the MAE is not effectively accessible to cumulus convection. The “vertical part” of the MAE, however, can be a source of kinetic energy for cumulus convection. Thus, the concept of MAE can be applied to a column of air to measure the convective instability that it possesses. For such an air column, the “vertical component” of the MAE is a measure of the portion of total potential energy available for conversion into convective kinetic energy, and is similar to the Convective Available Potential Energy (CAPE). In next chapter, we will define such a quantity for an atmospheric column, as a measure of its CAPE, and compare the atmospheric instability as measured by this new method with those from other methods.

When we lift an air parcel to an arbitrary new level, if its density is greater than that of the surrounding air, it will tend to return to its original position. Such an atmosphere is said to be statically stable. Otherwise, if the density of the lifted parcel is less than that of the environmental air at the new level, the lifted parcel will be positively buoyant and will, therefore, tend to accelerate upward. In such a case, the atmosphere is statically unstable. The neutral state is the “boundary” between the stable and unstable states. In the neutral state, the density of lifted parcel is equal to that of the environmental air.

Since the approximation that a lifted air parcel has the same pressure as its surrounding environment can be used, we also can use the temperatures of a lifted parcel and environment to judge the static stability of the atmosphere. If the lifted parcel is warmer (colder) than its environment, it is lighter (heavier) than the environment, and therefore the atmosphere is statically unstable (stable). Strictly speaking, when we consider a moist atmosphere, virtual temperature should be used instead of temperature to measure the static stability.

Since the lapse rate represents the rate of temperature change with height, it can be used to measure the static stability of the atmosphere. For a dry atmosphere, if the lapse rate ( $\Gamma = -\frac{dT}{dz}$ ) is larger (cooling more rapidly upward) than the dry adiabatic lapse rate ( $\Gamma_d$ ), that is, if  $\Gamma > \Gamma_d$ ,



then an air parcel lifted dry-adiabatically will become warmer than its environment so that the atmosphere is statically unstable. Similarly, if  $\Gamma < \Gamma_d$ , the atmosphere is statically stable.

For a given pressure, air with a higher (lower) temperature has a higher (lower) potential temperature ( $\theta$ ). And also, for dry adiabatic motions, the  $\theta$  of a lifted parcel is conserved. This means that, for a dry atmosphere, by comparing the  $\theta$ 's of two parcels, we can determine which one will be warmer or colder at any given pressure level. The air with the higher  $\theta$  will be warmer than the air with lower  $\theta$ , when they are put at the same pressure. Therefore, the vertical derivative of  $\theta$  can be used as a measure of the static stability. When  $\frac{d\theta}{dz} > 0$ , the  $\theta$  of lower-level air is less than that of higher-level air, so when the lower-level air is lifted, it will be cooler than its environment. The atmosphere is therefore statically stable. Similarly, when  $\frac{d\theta}{dz} < 0$ , the atmosphere is statically unstable, and when  $\frac{d\theta}{dz} = 0$ , the atmosphere is statically neutral.

In reality, however, the atmosphere contains water vapor. When a parcel is lifted, it may become saturated, so that some water vapor condenses, and latent heat is released. The latent heating raises the temperature of the lifted parcel. The static stability criterion for a moist atmosphere is, therefore, different from that of a dry atmosphere.

One of the simplest concepts used in the analysis of a moist atmosphere is the “pseudoadiabatic” process, in which all condensed water is assumed to drop out as soon as it forms. The pseudoadiabatic lapse rate ( $\Gamma_s$ ) can be used to judge the static stability of the moist atmosphere. If the atmospheric lapse rate ( $\Gamma$ ) is larger (cooling more rapidly upward) than the pseudoadiabatic lapse rate ( $\Gamma_s$ ), that is,  $\Gamma > \Gamma_s$ , the atmosphere is statically unstable for pseudoadiabatic motions. Otherwise, if  $\Gamma < \Gamma_s$ , the atmosphere is statically stable for pseudoadiabatic motions.

It can easily be shown (e.g. Holton, 1979) that the dry-adiabatic lapse rate is always larger than the pseudoadiabatic lapse rate, that is,  $\Gamma_d > \Gamma_s$ , because of the latent heat of condensation. When an atmosphere is statically stable for dry adiabatic motions, it may be statically unstable for pseudoadiabatic motions. This is just the case in which the lapse rate lies between  $\Gamma_s$  and  $\Gamma_d$ ,



$\Gamma_s < \Gamma < \Gamma_d$ , so that the atmosphere is stable with respect to dry adiabatic displacements but unstable with respect to pseudoadiabatic displacements. Such an instability is referred to as “conditional instability.” The “condition” is the saturation of the lifted parcel.

In the real atmosphere, the lapse rate is rarely greater than the dry adiabatic lapse rate, so that the atmosphere is mostly statically stable for dry adiabatic processes. The most common type of static instability is the conditional instability. It can be shown (e.g. Holton, 1979) that  $\theta_e$ , the equivalent potential temperature, can be used approximately to define a criterion for the conditional stability. When  $\frac{\partial \theta_e}{\partial z} < 0$ , the atmosphere is unstable;  $\frac{\partial \theta_e}{\partial z} > 0$ , stable;  $\frac{\partial \theta_e}{\partial z} = 0$ , neutral.

If the atmosphere is statically unstable, a lifted moist parcel will obtain positive buoyancy and therefore convective kinetic energy. It is therefore convenient to measure the atmospheric instability by the convective kinetic energy that the parcel will obtain. The Convective Available Potential Energy (CAPE) is just such a measure. It represents the maximum possible kinetic energy that a lifted parcel can acquire in a conditionally unstable atmosphere. The kinetic energy that a lifted parcel can acquire is the work done by the buoyancy force, i. e.

$$CAPE = \int_{p_{NB}}^{p_{FC}} R_d (T_{v,p} - T_v) d \ln p. \quad (1.1)$$

Here  $p_{FC}$  is the pressure of the free convection level,  $p_{NB}$  is the pressure of the neutral buoyancy level,  $R_d$  is the specific gas constant of dry air,  $T_{v,p}$  is the virtual temperature of the lifted parcel, and  $T_v$  is the virtual temperature of the environment. CAPE is an energy-related measurement of convective instability. The cloud work function of Arakawa and Schubert (1974) is a similar energy-related concept. It also measures the kinetic energy that a lifted parcel can obtain through the work done by buoyancy. Unlike the CAPE, however, the cloud work function includes the effects of entrainment on buoyancy.

The above are the traditional methods to measure the static instability of the atmosphere or the convective kinetic energy that a lifted parcel can acquire in a statically unstable atmosphere. One of the basic assumptions of these methods is that the lifted parcel is small enough so that its



displacement does not disturb the surrounding environment. In reality, however, the rising motion must be compensated for by subsidence in the environment, if an overall mass balance is to be maintained. The dry environment between the cloudy updrafts must descend, so that the environment is in fact disturbed. Thus, we should try to take into account the changes of the environment when the instability of the atmosphere is considered.

Bjerknes (1938) first included the effects of the environmental air in the computation of conditional instability. He calculated the conditional instability of the adiabatic ascent of saturated air through a dry-adiabatically descending environment. He assumed that on any horizontal plane the upward mass flux in convection cells is just balanced by the downward mass flux in the cloudless environment. The saturated air ascends adiabatically, while the environment descends dry-adiabatically. He showed that the net heating for a layer can be expressed as the sum of two terms, one representing the released latent heat of condensation in clouds, and the other representing the dry-adiabatic warming due to the downward compensating flow. The latent heat of condensation in clouds was considered to be the only source of convective kinetic energy.

Because of the warming of the environment due to the compensating dry-adiabatic descent, a rising parcel must be heated more than if the environment were undisturbed, in order to obtain a given amount of buoyancy. Bjerknes' results showed that in order for the rising cloudy parcel to obtain positive buoyancy, the cloudy tower must be narrow enough. That is, convective clouds are likely to occur in a system with appreciable upward velocity in narrow cloud towers and slow downward motion in the wide cloudless spaces. How narrow the cloudy area must be, compared to the cloudless area, depends on the lapse rates of the observed sounding and the dry- and saturated-adiabatic processes.

Bjerknes also compared two measures of convective instability, i.e., the classical method in which an infinitely small parcel does not disturb its environment, and his method in which finite cloud towers lead to environmental sinking. For this purpose, he used an ordinary sounding. For such a sounding, when a parcel is lifted saturated-adiabatically from its saturation level to a point



above, the parcel method shows that the lifted parcel will have positive buoyancy and gain convective kinetic energy; but Bjerknes method shows that the finite lifted parcel will have negative buoyancy and cannot obtain convective kinetic energy at all. Bjerknes also did other comparisons between the two methods. His conclusion is that the atmosphere is always less unstable with respect to a system of finite cloud towers than with respect to the infinitely small saturated parcels.

As has been shown by Bjerknes, the effects of compensating return flow between clouds can change our conclusion about the degree of convective instability. Although Bjerknes showed the importance of including the compensating return flow, he did not quantitatively show how to measure the convective instability with the return flow included. We will show in next chapter that the method that we propose does include the effects of compensating return flow quantitatively for measuring convective instability of the atmosphere.

In addition, the previous parcel-lifting methods for measuring the convective kinetic energy (e.g., CAPE, cloud work function) depend on the choice of the parcel lifted. For different lifted parcels, the measured instability may be different. This can be clearly seen, for instance, from the definition of CAPE, (1.1). It shows that the CAPE is the total work done by buoyancy when a parcel is lifted. The value of this work is the product of two factors: the buoyancy that the lifted parcel experienced, and the length of the path over which the parcel has positive buoyancy. If a warmer and wetter parcel is lifted, it will have more buoyancy and its path will be longer, so its CAPE will be larger than that of a colder and / or drier parcel. This shows that for a given sounding, lifting different parcels can give different CAPEs. It is clearly desirable to have a unique value of CAPE for a given sounding. We will show that our measure of the convective instability is unique. It is a property of a whole atmospheric column, and does not make reference to any particular lifted parcel.

Cumulus convection, especially deep and intense convection, is one of the major processes affecting the dynamics and energetics of large-scale atmospheric circulations. The ways through which convection exerts influence include: diabatic heating due to latent heat release in penetra-



tive cumulus convection; vertical transports of heat, moisture and momentum; and the interaction of cumulus clouds with radiation. Riehl and Malkus (1958) showed the importance of cumulus convection for the heat balance of the tropical atmosphere. They showed that deep cumulus convection carries the released latent heat of condensation to the upper troposphere, to balance radiative cooling there.

The role of deep convection in the formation and growth of tropical cyclones was discussed by Riehl and Malkus (1961), Yanai (1961a,b), Ooyama (1964), and Charney and Eliassen (1964). Their results showed that tropical cyclones largely owe their existence to the release of latent heat in cumulus convection. They also showed that, to appropriately explain the growth of tropical cyclones in any model, cumulus heating must be adequately parameterized in the framework of the large-scale motion.

Cumulus convection is thus very important for the large-scale flow. It is necessary to account for these effects in a quantitative way in models of large-scale circulations. Ideally, if the resolution of models were sufficiently fine, individual clouds and their effects on the environment could be calculated directly, so that we would not need to parameterize them. To do so, however, horizontal and vertical grid sizes of between 100 and 1000 m would be required (Cotton and Anthes, 1989). Such a high resolution covering the domain size necessary to simulate larger-scale phenomena is far beyond present and foreseeable computational capability. The problem of cumulus parameterization will, therefore, remain important in any foreseeable future. Even with sufficient computer power, cumulus parameterization is still useful for understanding. Moreover, demands for simple numerical or theoretical models always exist regardless of computer power.

Before parameterizing the effects of cumulus convection, we need a thorough understanding of the structure and dynamics of individual clouds and the micro behavior of these clouds. Unfortunately, our knowledge of clouds is quite limited, because the transports of mass, moisture, heat and momentum by clouds are not directly measured. Instead, we only can estimate what these transports must be in order to account for the residuals in the large-scale budget equations.



To do so, a diagnostic cumulus cloud ensemble model must be employed and therefore, the results are model-dependent.

Yanai *et al.* (1973) performed the first such study to determine the bulk properties of tropical cloud clusters from the large-scale heat and moisture budgets, using the Marshall Islands data. A bulk model was used. In this model, clouds were classified according to the heights of their tops, and all clouds were assumed to have the same cloud base. A system of equations, based on consideration of the cloud properties and the cloud effects on the large-scale fields, was solved to obtain the averaged cloud properties. The vertical profiles of these quantities describe the mean structure of the cumulus ensemble and the net effects of the clouds on their environment. The results showed that the upward mass flux in active cumulus clouds is larger than that required from large-scale horizontal convergence, thus causing a compensating sinking motion between active clouds. Entrainment, which is the mass added into the cloud from the environment from the side and / or the top of the cloud, was shown to be strongest in the lower troposphere, while detrainment, which is the mass carried away from the cloud into the environment from the sides and / or the top, has strong maxima in both the lower and upper troposphere. The lower detrainment maximum suggests the existence of a large number of shallow cumulus clouds in the region, co-existing with deep cumulus clouds. The large-scale heating of the environment by cumulus clouds was found to be primarily due to the adiabatic compression due to compensating downward motion. The cooling due to re-evaporation of liquid water detrained from clouds is also an important factor in the heat balance of the environment. The environment was found to be mostly dried by deep convection, due to the downward compensating flow between clouds. Counteracting the drying due to the environmental sinking motion are the large amount of water vapor and liquid water which are detrained from clouds, especially from the shallow clouds in the lower troposphere.

Also using the Marshall Islands data, Ogura and Cho (1973) applied a model of a cumulus ensemble to determine the cloud properties and the cloud contributions to the changes of heat and



moisture content of the large-scale environment, from the large-scale budgets. Unlike the cumulus ensemble model of Yanai *et al.* (1973), which only estimated the average properties of the clouds, the Ogura-Cho model employed a spectral cloud model so that the properties of different cloud types could be found. This is one important advantage of the spectral model over the bulk model. The key point in the spectral model is that the properties of a single cloud are uniquely determined by an entrainment parameter, so that, by distinguishing the entrainment parameters, different cloud types can be distinguished. Arakawa and Schubert (1974) discussed the same spectral cloud model. The results of Ogura and Cho (1973) are basically the same as those of Yanai *et al.* (1973), except that the contributions from different cloud types can be seen.

As we have mentioned before, some observational studies showed the existence of downdrafts in cumulus clouds as early as the 1940's and 1950's (e.g., Byers and Hull, 1949; Squires, 1958). When we use cloud models to determine the properties of clouds, the effects of downdrafts should be included. Johnson (1976) incorporated downdrafts into the spectral cloud model. He assumed that each individual cloud element possesses an updraft and downdraft that are steady, entraining plumes, and that a constant ratio exists between the intensities of the updraft and downdraft. His results showed that the neglect of cumulus downdrafts and their associated rainfall evaporation leads to excessively large populations of shallow cumulus clouds in the highly convective situations. Nitta (1977) obtained the same conclusions by using an improved treatment of downdrafts in the spectral cloud model.

Since cumulus convection has important effects on larger-scale motions, and the grids of the large-scale models can not resolve the cumulus activity, we must find a way to relate the effects of the "subgrid-scale" cumulus clouds to the motions resolvable to the models. This is known as cumulus parameterization. For cumulus convection to be parameterizable, it is necessary that the convection be controlled by the large-scale motions. Many observations show that the large-scale processes do control convection.

According to Cotton and Anthes (1989), one of the first observational studies that showed



a strong dependence of deep cumulus convection on larger-scale variables in the tropics was by Malkus and Williams (1963). They found that deep cumulus convection occurs only where low-level synoptic scale convergence prevails. They also noted that dynamic, rather than thermodynamic, factors are more crucial for cloud growth in the tropics, and that deep convection is characterized by marginal instability and low-level convergence, while very fair conditions are characterized by much stronger instability and divergence. These early observations were later confirmed by other studies (Matsumoto *et al.*, 1967; Cho and Ogura, 1974).

In addition, Cho and Ogura (1974) found a high correlation between the vertical mass flux in the deep clouds and the large-scale mass flux at 950 mb, for the composite wave data in the equatorial western pacific. Yanai *et al.* (1976) showed that deep cumulus clouds in the Marshall Islands region were highly correlated with the large-scale vertical motion in the upper troposphere. Nitta (1978) also showed that deep cumulus convection over the Global Atmosphere Research Program's Atlantic Tropical Experiment (GATE) area was highly correlated with the large-scale vertical velocity at all levels.

For the extratropics, there is also a lot of observational evidence showing that cumulus convection is strongly controlled by large-scale processes. For example, Sasaki and Lewis (1970), Lewis (1971), and Hudson (1971) found a close agreement between active convection and areas of mass and moisture convergence over the central United States. All of this observational evidence that deep convection is influenced and controlled by the large-scale motions provides a physical basis for cumulus parameterization, and implies that it is possible to parameterize the effects of cumulus convection in both the tropics and extratropics.

One of the purposes of cumulus parameterization is to determine the total net rate of condensation, and to distribute the convective heating and moistening vertically. Since the convective processes are subgrid scale, all cumulus parameterizations require closure assumptions. Since observations show that deep convection is invariably related to upward vertical motions and low level convergence, some authors have assumed that the large-scale vertical motion at the top of



boundary layer and the low level convergence of mass and water vapor are proportional to some measure of the convective activity. Also, cumulus convection acts to release the convective instability in the atmosphere, so as to modify a conditionally unstable atmosphere toward a more stable state. If the approximate end-state can be specified, this can provide a convenient basis for estimating the intensity of convection. This is the basis of the moist convective adjustment scheme.

The moist convective adjustment (MCA) schemes (Manabe *et al.*, 1965; Miyakoda *et al.*, 1969; Krishnamurti and Moxim, 1971; Kurihara, 1973) are the simplest cumulus parameterizations. In MCA, it is assumed that deep moist convection acts to restore the lapse rate to a neutral or stable condition, and that there exists a critical temperature and moisture profile associated with the neutral or stable state. When the large-scale sounding becomes more unstable than this critical state, it is adjusted toward the critical state. This stabilization is assumed to be caused by cumulus convection.

The MCA schemes can be separated into hard and soft varieties. In the hard convective adjustment (according to Krishnamurti *et al.*, 1980), if some portion of a given column is convectively unstable, that is  $\partial\theta_e/\partial z < 0$  for that region (where  $\theta_e$  is the equivalent potential temperature), only this portion of the sounding needs to be adjusted to eliminate the instability. The value of the moist static energy ( $h = gz + c_p T + Lq$ ) of the adjusted portion of the sounding must be the average moist static energy of the initial sounding over the unstable layer, in order to ensure energy conservation during the adjustment. Hard convective adjustment produces unrealistic modifications of the large-scale sounding by excessively cooling and drying the lower troposphere, and producing too much precipitation.

Because of the problems associated with the hard convective adjustment schemes, efforts have been made to improve them, e. g., by producing much slower and more realistic adjustment. Such methods are known as soft adjustment schemes. One of the soft schemes assumptions, according to Krishnamurti *et al.*(1980), is that the hard adjustment occurs over a fraction  $\sigma$  of the grid-scale area. Over the remaining area  $(1 - \sigma)$  it is assumed that the vertical profiles of temper-



ature and humidity remain invariant during the time step. The final sounding in the  $\sigma$  region is determined from the construction of a moist adiabat. Then the final temperature and mixing ratio on the grid scale are just the average of those in the two regions,  $\sigma$  and  $(1 - \sigma)$ . Although this represents an improvement over the hard convective adjustment, because of the occurrence of the maximum instability before the time of maximum convection in the tropics, the soft adjustment scheme shows a lag of 1 to 2 days between the calculated and observed precipitation. This large lag makes the soft adjustment scheme a poor choice when the timing of precipitation is important.

Kuo (1965, 1974) designed a cumulus parameterization based on the relationship between convective rainfall and large-scale moisture convergence. Since observational studies have shown that there is a strong correlation between the observed convective rainfall and the total large-scale convergence of water vapor in the column, Kuo chose the large-scale moisture convergence rate as a key variable to parameterize the effects of convection in large-scale models. Parameterizations (Kuo, 1965, 1974; Anthes 1977; Krishnamurti *et al.*, 1976, 1980, 1983; and Molinari, 1982) based on large-scale moisture convergence are called Kuo schemes. Basically, Kuo (1974) assumed that a fraction,  $(1-b)$ , of the total water vapor converge is condensed and precipitated, and so heats the column, while the remaining fraction,  $b$ , is stored and acts to increase the humidity of the column. Determination of  $b$  is obviously an important aspect of the Kuo scheme. Several methods have been proposed to determine  $b$ , by different authors. The vertical profiles of convective heating and moistening are based on the assumption that environment is modified through the mixing of cloudy air and the environmental air. The convective condensation heating and moistening are, therefore, directly proportional to the local excess of cloud temperature and moisture over the corresponding environmental values. The cloud temperature and moisture content can be calculated from moist adiabatic processes, although they also can be calculated from a cloud model (Anthes, 1977). The results of the Kuo scheme are much improved over those of the moist adjustment schemes, and therefore, the Kuo scheme has been popular.

An advantage of Kuo's scheme is that it provides immediate measures of cumulus-scale



heat and moisture fluxes in terms of the measurable large-scale variables, without having to compute cloud dynamical processes and cloud microphysical processes. On the other hand, however, the simplicity of the Kuo scheme makes it impossible to see explicitly the interactions between cumulus clouds and the large-scale motions. Also because of the simplicity, many factors have to be determined empirically. Whereas convection is strongly controlled by the large-scale convergent flow in the tropics, it seems to have less significance in the extratropics (Frank, 1983; Tiedtke, 1989). This makes applications of the Kuo scheme in the extratropics questionable. More importantly, objections have been raised against Kuo's assumption that the environment is heated by the mixing of cloud air with the environmental air. As has been shown by Yanai *et al.* (1973), Ogura and Cho (1973), cumulus convection interacts with environment mainly through cumulus-induced subsidence in the environment between clouds, rather than through the mixing of cloud air with the environmental air.

Arakawa and Schubert (1974) developed a sophisticated cumulus parameterization scheme which includes many physical processes. In the Arakawa-Schubert (AS) scheme, a spectrum of cloud types is considered, so that the effects of different cloud types can be seen explicitly. Also, the AS scheme relates convective clouds to the large-scale forcing, which involves horizontal and vertical advection, radiation, and the surface fluxes of heat and moisture, rather than only large-scale moisture convergence as in the Kuo scheme. In particular, the AS parameterization makes the use of the assumption that the real atmosphere is in a quasi-equilibrium state, in which the rate of destabilization by large-scale processes and the rate of stabilization by cumulus convection almost balance each other. That is, the large-scale forcing produces convective clouds, and the clouds consume the instability caused by the large-scale forcing, making the atmosphere stay close to an equilibrium state in which the instability of the atmosphere remains nearly unchanged. In this way, the AS parameterization is an adjustment scheme. The intensity of convection, expressed in terms of the cloud mass flux, is determined by the large-scale forcing. Then, through the spectral cloud model, other cloud properties can be determined. With these cloud properties known, the effects of cumulus convection on the environment can be determined. The



AS scheme assumes that an ensemble of cumulus clouds affects its environment in two major ways: (1) by inducing subsidence between clouds, which warms and dries the environment; and (2) through detrainment of the saturated air, which contains liquid water or ice, from cloud top. Evaporation of the detained cloud water causes cooling and moistening of the environment.

Since the AS scheme relates cloud activity to the total large-scale forcing, not just the large-scale water vapor convergence as in the Kuo scheme, it is more realistic. The AS scheme is also appealing because of its clear physical concept of the interaction of cumulus clouds and the large-scale environment. In this respect it is presently not matched by any other scheme.

An obvious disadvantage of the AS scheme, however, is its complexity, which makes it more difficult to implement into large-scale models, and computationally more expensive. Although the key assumption of AS scheme, the quasi-equilibrium hypothesis, has received considerable support from observations (e.g., Lord and Arakawa, 1980; Lord 1982; Arakawa and Chen, 1987; Xu and Emanuel, 1989) and numerical simulations (e.g., Ogura and Kao, 1987; Kao and Ogura, 1987; Grell *et al.*, 1991; Xu and Arakawa, 1992), there are still some questions about the validity of the quasi-equilibrium assumption for mesoscale and non-slowly varying fields (Frank, 1983; Tiedtke, 1989). Besides, the AS scheme assumes that the instability increase due to the large-scale processes will immediately be released by convection, so that the atmosphere will not increase its instability. This means that the AS scheme cannot predict the instability stored in the weather system. In the middle latitudes, however, sometimes the instability produced by large-scale processes can be stored in the atmosphere without triggering convection. Using the AS scheme in forecasting models for such cases will not produce accurate results.

Betts (1986), Betts and Miller (1986) presented another cumulus parameterization in which the main assumption is that when the sounding shows some kind of convective instability, it is adjusted by convection toward a quasi-equilibrium reference state. This scheme therefore belongs to the moist adjustment type schemes. However, in contrast to the previous adjustment schemes, the adjustment profiles have been chosen to represent the thermodynamic structures



which are typically observed in convective situations and which resemble quasi-equilibrium states between the large-scale forcing and cumulus convection. Another important difference between the Betts-Miller scheme and the traditional adjustment schemes is that the adjustment is applied over a finite time interval, which makes the scheme a relaxation scheme. These two critical differences make the results from this scheme much better than those of the traditional adjustment schemes (Tiedtke, 1989). Also, the scheme is very simple, since all it needs are the specified reference profiles, the relaxation time, and a criterion for activating the scheme.

The key limitation of the Betts-Miller scheme is the definition of the reference profiles. Betts and Miller (1986) specified the reference profiles empirically from observed soundings. It is impossible that the reference profiles are unique; they must differ from region to region and may also depend on the synoptic situation. In addition, as mentioned before, the quasi-equilibrium assumption may be valid only for slowly varying fields but not for faster systems, making the scheme not applicable in meso-scale models. Also, as for most other adjustment schemes, the interactions between cumulus clouds and the large-scale processes are not explicitly shown.

Since penetrative downdrafts have been shown to make important contributions to the large-scale heat and moisture budgets (Johnson, 1976, 1980; Nitta, 1977, 1978), their effects were included in most of the cumulus parameterization schemes mentioned above (e. g., Cheng and Arakawa, 1990; Betts and Miller, 1993), as revisions of the original schemes.

We defined a Generalized Convective Available Potential Energy (GCAPE), and devised a parcel-moving algorithm for calculating it. The GCAPE of GATE data and ASTEX data were calculated, and the effects of ice were included. We found a high positive correlation between the rate of GCAPE production by large-scale processes and the observed precipitation rate, while a negative correlation exists between the GCAPE itself and the precipitation rate. The time change rate of observed GCAPE is much smaller than the GCAPE production rate by large-scale processes, implying that the real atmosphere stays close to a neutral state.



We also devised a penetrator algorithm, in which mass transport occurs in penetrative updrafts (downdrafts) with compensating layer-by-layer sinking (rising) motion. The solution was obtained using nonlinear optimization theory. Our results show that the penetrator algorithm is more effective than the Lorenz algorithm, in certain respects. It detects more GCAPE, and does not require high vertical resolution. The liquid water / ice distribution within reference-state cloud layers obtained with the penetrator algorithm is much smoother than that obtained with the Lorenz algorithm. Downward penetrators have been detected, but our results show that their contribution is much smaller than that of the upward penetrators.

Recently, we have formulated a cumulus parameterization scheme based on the concept of GCAPE. The equilibrium state to which the parameterization adjusts is the reference state used in the definition of the GCAPE. An attractive aspect of this approach is that the equilibrium state is based neither on empiricism nor on simple cloud models, but rather on the basic physics of moist available potential energy. This is being discussed in a conference paper by Wang and Randall (1994) at the Numerical Weather Prediction Conference of the American Meteorological Society in Portland, Oregon.

Additional information about our research and the results we have obtained is given in the attachments.

## **II. Human resources**

This project supported a graduate student, J. Wang, who successfully defended his Ph.D. thesis in early 1994.

## **III. Publications resulting from this project**

Wang, J., and D. A. Randall, 1991: The Moist Available Energy of a Conditionally Unstable Atmosphere. Paper presented at the *19th Conference on Hurricanes and Tropical Meteorology of the American Meteorological Society*, Miami, Florida.

Randall, D. A., and J. Wang, 1991: The moist available energy of a conditionally unstable atmosphere. *Journal of the Atmospheric Sciences*, **49**, 240-255.



- Wang, J., 1994: *Generalized Convective Available Potential Energy and Its Application to Cumulus Parameterization*. Ph.D. dissertation, Colorado State University.
- Wang, J., and D. A. Randall, 1994: The moist available energy of a conditionally unstable atmosphere, II: Further analysis of the GATE data. *Journal of the Atmospheric Sciences*, **51**, 703-710.
- Wang, J., and D. A. Randall, 1994: A cumulus parameterization based on the concept of GCAPE. Paper presented at the *Tenth Conference on Numerical Weather Prediction of the American Meteorological Society*, Portland Oregon.

In addition to the publications listed above, we anticipate that one more journal article will be written based on the results of this project.







**Attachments:**

Randall, D. A., and J. Wang, 1991: The moist available energy of a conditionally unstable atmosphere. *Journal of the Atmospheric Sciences*, **49**, 240-255.

Wang, J., 1994: *Generalized Convective Available Potential Energy and Its Application to Cumulus Parameterization*. Ph.D. dissertation, Colorado State University (cover page and abstract only).

Wang, J., and D. A. Randall, 1994: The moist available energy of a conditionally unstable atmosphere, II: Further analysis of the GATE data. *Journal of the Atmospheric Sciences*, **51**, 703-710.



## The Moist Available Energy of a Conditionally Unstable Atmosphere

DAVID A. RANDALL AND JUNYI WANG

*Department of Atmospheric Science, Colorado State University, Fort Collins, Colorado*

(Manuscript received 16 October 1990, in final form 1 July 1991)

### ABSTRACT

The concept of "moist available energy," defined by Lorenz, is applied to study the potential energy available for cumulus convection in a conditionally unstable atmosphere. A modified version of Lorenz's parcel-moving algorithm is applied to the GATE data to determine the time variations of the moist available energy of the observed tropical atmosphere. Lorenz's algorithm is found to be somewhat impractical, and a new algorithm based on mass exchanges is proposed. Implications for cumulus parameterization are discussed.

### 1. Introduction

Conditional instability is a concept that is familiar to every first-year meteorology student. The methods that are used to detect conditional instability in observed or simulated soundings typically involve consideration of the potential energy that can be released when a parcel is displaced vertically. The parcel's level of origin is usually chosen somewhat arbitrarily, and the possibility of multiple parcels originating at multiple levels is usually not admitted. The response of the parcel's environment is usually not taken into account.

We need a method to determine the potential energy available for cumulus convection without such restrictive and arbitrary assumptions. The purpose of this paper is to show that Lorenz's (1978) concept of "moist available energy" holds the key to such a method.

Lorenz (1955) defined the available potential energy (APE) of the atmosphere as the difference between the actual total enthalpy and the minimum total enthalpy that could be achieved by rearranging the mass under reversible adiabatic processes.

This definition can be understood by considering the conservation equation for the total energy of the atmosphere (including the internal, potential, and kinetic energies). According to this equation, the sum of the kinetic energy per unit mass and the enthalpy per unit mass changes in time due to redistribution of mass within the atmosphere, and also due to energy sources and sinks such as radiation, latent heating, and surface exchanges. Here the enthalpy per unit mass is defined as the product of the temperature and the specific heat at constant pressure. Of course, when the

total energy equation is integrated over the entire atmosphere, the redistribution term drops out. In the absence of energy sources or sinks, therefore, we find that

$$\frac{\partial}{\partial t} (K + H) = 0, \quad (1.1)$$

where  $K$  is the total kinetic energy, and  $H$  is the total enthalpy.

The total enthalpy can be varied by adiabatically redistributing mass over the globe, and Lorenz pointed out that there exists a particular mass distribution for which  $H$  is minimized. According to (1.1),  $K$  is maximized for this same state, which Lorenz called the *reference state*. The APE is then defined as the difference between the total enthalpy of the given state and that of the reference state. It thus represents the portion of the nonkinetic energy that is available for conversion into kinetic energy under reversible adiabatic processes.

Lorenz (1978, 1979; hereafter L78 and L79, respectively) extended the concept of APE to the moist atmosphere by recognizing that moist adiabatic processes are, in fact, adiabatic rather than diabatic. From this point of view, the latent heat of water vapor is a portion of the enthalpy. He presented both graphical and digital algorithms for determining the moist available energy. The latter was based on rearranging discrete parcels from their configuration in the given state to that in the reference state. He showed that the moist available energy (MAE) is never less than the dry available energy (DAE, synonymous with the dry APE), although the DAE represents the bulk of the total available energy in the global atmosphere. He demonstrated that for fixed relative humidity the MAE increases rapidly as the temperature increases. He was also able to define a specific MAE, i.e., the contribution of a particular parcel to the global MAE. The fact that the MAE is an

*Corresponding author address:* Dr. David A. Randall, Department of Atmospheric Science, Colorado State University, Fort Collins, CO 80523.

upper bound on the amount of kinetic energy that can be generated by any circulation whatsoever is both a strength and a weakness. It is a strength because the concept is completely general. It is a weakness because it is possible that no dynamically realizable circulation can extract all of the available energy.

The concept of available energy is usually applied to statically stable atmospheric states, but it is equally applicable to statically unstable systems. When the atmosphere is everywhere statically stable in the dry sense, the DAE is entirely due to the existence of temperature gradients along isobaric surfaces, i.e., the DAE resides in the horizontal rather than the vertical structure of the atmosphere. The reference state can be reached by rearranging the mass of the system so that the pressure is uniform along isentropic surfaces. The vertical ordering of the isentropic surfaces does not change during this process. For a dry statically unstable system, on the other hand, the reference state can only be reached by vertically reordering the isentropes; the potential temperature decreases upward in the given state, but increases upward in the reference state.

As an example, consider a simple system containing two parcels of equal mass. In the given state, parcels with potential temperatures  $\theta_1$  and  $\theta_2$  reside at pressures  $p_1$  and  $p_2$ , respectively. We assume that  $\theta_1 < \theta_2$  and  $p_1 < p_2$ , so that the given state is statically unstable. The enthalpy per unit mass of parcel  $i$  is  $c_p\theta_i(p_i/p_0)^\kappa$ , where  $p_0$  is the reference pressure used in the definition of the potential temperature, and  $\kappa$  is Poisson's constant. If the parcels are interchanged ("swapped") so that parcel number 2 goes to pressure  $p_1$  and vice versa, the change in the total enthalpy per unit mass is  $c_p(\theta_1 - \theta_2)[(p_2/p_0)^\kappa - (p_1/p_0)^\kappa]$ , which is negative. This implies that the total enthalpy is minimized by the swap; the final state is the reference state, and the change in enthalpy given above is the available potential energy of the system.

The moist atmospheres used as examples in L78 and L79 were statically stable everywhere; for such atmospheres, the MAE resides in the horizontal rather than the vertical structure. Lorenz did point out, however, that the existence of conditional instability represents a supply of MAE and complicates the design of algorithms to determine the MAE. Consider an idealized atmosphere that is horizontally homogeneous but conditionally unstable. Since the dry static stability is positive, the DAE is zero, but the MAE is positive. When the given state is conditionally unstable, a portion of the air in the reference state must be saturated.

Of course, the real atmosphere is horizontally inhomogeneous and contains local regions of conditional instability. The MAE of the real atmosphere resides, therefore, partly in the atmosphere's horizontal structure and partly in its vertical structure. For convenience, we say that the MAE has both horizontal and vertical "components." The vertical component of the MAE is a generalization of the convective available

potential energy (CAPE); to distinguish it from Lorenz's globally defined MAE, we refer to the local vertical component of the MAE as the generalized CAPE, or GCAPE.

The GCAPE is converted into the kinetic energy of cumulus convection on the relatively fast time scale of the convection itself—on the order of an hour or at most a few hours (e.g., Lord and Arakawa 1980; Soong and Tao 1980; Krueger 1988; Dudhia and Moncreif 1988; Xu 1991). As a result, the convectively active atmosphere never strays far from conditional neutrality (e.g., Arakawa and Schubert 1974; Xu and Emanuel 1987); the GCAPE is consumed as rapidly as it is generated by such processes as large-scale rising motion, radiative cooling, moisture convergence, and surface evaporation. In contrast, the horizontal component of the MAE is inaccessible to cumulus convection but can be released by such relatively slow mechanisms as baroclinic instability, with time scales on the order of a few days.

In short, there is a great difference in time scale between the cumulus circulations that draw on the GCAPE and the synoptic circulations that draw on the horizontal component of the MAE. Because of this scale separation, it is useful to distinguish between the horizontal and vertical components of the MAE. In particular, *the dynamical processes that tend to increase or decrease the GCAPE can be considered separately from those that tend to increase or decrease the portion of the available potential energy that resides in the horizontal structure of the atmosphere.* In a sense, this is a basic premise of all cumulus parameterization the-

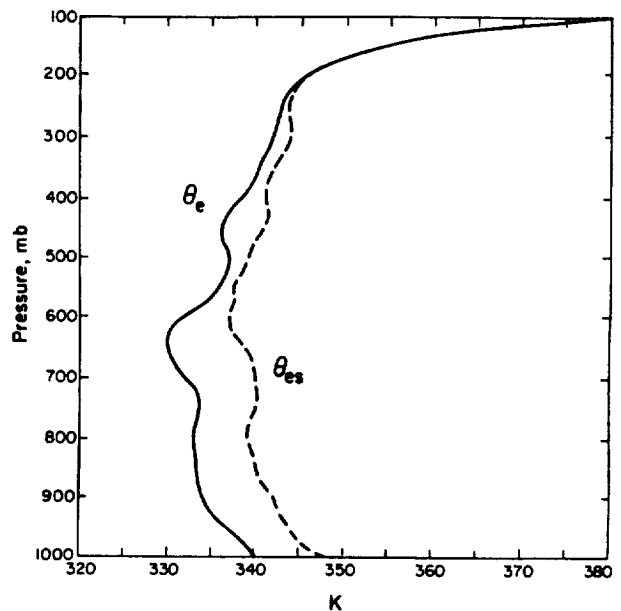


FIG. 1. Observed soundings of equivalent potential temperature (solid line) and saturation equivalent potential temperature (dashed line) for GATE Phase III, 1800 UTC 30 August.

ories (Arakawa and Schubert 1974). The purpose of this paper is to investigate the GCAPE of conditionally unstable soundings and its possible relevance to the problem of cumulus parameterization.

## 2. The GCAPE of GATE soundings

We have computed the GCAPE of GATE soundings, as analyzed by Thompson et al. (1979), using a modified version of the parcel-moving (PM) algorithm discussed by L79. The data used here, kindly provided by R. Reed, consist of a single sounding for each of 157 GATE Phase III observation times. The thermodynamic formulas used are given in appendix A, while the PM algorithm itself is described in appendix B. We also tested a "brute force" method, which checks all possible permutations of the parcels and selects the permutation for which  $H$  is minimized. This approach is feasible only when the number of parcels under con-

sideration is less than about 10. In order to apply the PM algorithm, each sounding is divided into  $N$  parcels; initially  $N = 9$  was used.

To our initial surprise, all of the GATE soundings tested were found to have zero GCAPE, i.e., the given states were the same as the reference states. This result was obtained with both the PM and brute force algorithms. An example of such a sounding, for 1800 UTC 30 August, is given in Fig. 1. It is clear that conditional instability exists, so that GCAPE *must* be present. At first, a programming error was suspected.

After further investigation, we determined that the reason that many of the GATE soundings were found to have no GCAPE at all is simple enough: the parcels that were being moved around, which ranged in size from about 30 mb to about 100 mb, were too massive. The problem with such massive parcels can be understood through the following argument. In convectively active situations, the cumulus mass flux is typically on

TABLE 1. Results of the parcel-moving method for GATE observation time 71. Here RH is the relative humidity. The GCAPE is 11.12 J kg<sup>-1</sup>.

Level	Given sounding						Reference sounding							
	$p$ (mb)	$T$ (K)	$\bar{w}$ (g kg <sup>-1</sup> )	RH (%)	$\theta_e$ (K)	$p_{max}$ (mb)	$p$ (mb)	$T$ (K)	$\bar{w}$ (g kg <sup>-1</sup> )	RH (%)	$\theta_e$ (K)	$\bar{w} - w$ (g kg <sup>-1</sup> )	$T_R - T$ (K)	$\bar{w}_R - \bar{w}$ (g kg <sup>-1</sup> )
1	112.5	197.3	0.008	67.7	368.28	106.78	112.5	197.3	0.008	67.7	368.28	.000	0.00	0.00
2	137.5	201.6	0.008	41.3	355.24	121.94	137.5	201.6	0.008	41.3	355.24	.000	0.00	0.00
3	162.5	207.3	0.014	40.1	348.30	142.87	162.5	210.8	17.05	30.936.9	348.32	16.993	13.53	17.03
4	187.5	213.3	0.028	42.5	344.13	165.41	187.5	215.9	0.014	15.3	348.30	.000	2.59	-0.01
5	212.5	219.7	0.051	40.7	341.98	185.30	212.5	221.1	0.028	18.8	344.13	.000	1.38	-0.02
6	237.5	225.9	0.096	41.9	340.56	206.98	237.5	226.8	0.051	20.3	341.98	.000	0.94	-0.04
7	262.5	231.7	0.130	33.7	339.44	220.03	262.5	232.4	0.096	22.9	340.56	.000	0.77	-0.03
8	287.5	237.2	0.223	36.0	338.63	242.18	287.5	237.8	0.130	19.8	339.44	.000	0.58	-0.09
9	312.5	242.1	0.285	30.9	337.56	255.37	312.5	242.9	0.223	22.5	338.63	.000	0.78	-0.06
10	337.5	246.4	0.335	26.4	336.06	267.24	337.5	247.5	0.285	20.2	337.56	.000	1.11	-0.05
11	362.5	250.3	0.422	25.1	334.52	283.15	362.5	251.5	0.335	18.0	336.06	.000	1.16	-0.09
12	387.5	254.0	0.617	28.5	333.03	308.02	387.5	255.1	0.422	17.7	334.52	.000	1.16	-0.20
13	412.5	257.3	0.931	34.4	331.54	337.74	412.5	258.5	0.617	20.6	333.03	.000	1.20	-0.31
14	437.5	260.4	1.338	40.8	329.97	368.39	437.5	261.7	0.931	25.5	331.54	.000	1.30	-0.41
15	462.5	262.9	1.972	51.8	328.08	406.46	462.5	264.5	1.338	30.9	329.97	.000	1.60	-0.63
16	487.5	265.0	2.946	69.1	325.95	452.63	487.5	266.9	1.972	40.0	328.08	.000	1.88	-0.97
17	512.5	267.1	3.774	79.6	323.91	489.23	512.5	268.9	2.946	54.2	325.95	.000	1.80	-0.83
18	537.5	269.0	4.578	87.4	322.01	522.70	537.5	270.7	3.774	63.3	323.91	.000	1.71	-0.80
19	562.5	270.7	5.225	91.5	320.04	552.17	562.5	272.5	4.578	70.3	322.01	.000	1.76	-0.65
20	587.5	272.5	5.806	93.0	318.30	578.53	587.5	274.1	5.225	74.5	320.04	.000	1.58	-0.58
21	612.5	274.6	6.329	90.9	317.01	600.19	612.5	275.8	5.806	76.5	318.30	.000	1.20	-0.52
22	637.5	276.6	7.209	93.2	315.88	627.95	637.5	277.8	6.329	75.5	317.01	.000	1.13	-0.88
23	662.5	278.5	7.584	89.4	314.59	646.64	662.5	279.7	7.209	78.2	315.88	.000	1.20	-0.38
24	687.5	280.3	8.204	88.3	313.45	669.05	687.5	281.4	7.584	75.6	314.59	.000	1.12	-0.62
25	712.5	282.0	8.766	87.0	312.27	690.85	712.5	283.2	8.204	75.2	313.45	.000	1.16	-0.56
26	737.5	283.6	8.719	80.3	310.97	702.38	737.5	284.8	8.766	74.5	312.27	.000	1.18	0.05
27	762.5	285.2	8.730	74.7	309.75	714.59	762.5	286.3	8.719	69.2	310.97	.000	1.13	-0.01
28	787.5	286.5	8.456	68.7	308.23	724.22	787.5	287.8	8.730	64.8	309.75	.000	1.36	0.27
29	812.5	287.5	9.172	71.9	306.71	754.47	812.5	289.0	8.456	59.9	308.23	.000	1.54	-0.72
30	837.5	288.6	10.67	80.4	305.48	796.96	837.5	290.0	9.172	63.0	306.71	.000	1.41	-1.50
31	862.5	289.8	11.51	82.8	304.32	825.99	862.5	291.0	10.67	70.7	305.48	.000	1.25	-0.85
32	887.5	291.2	12.63	85.4	303.52	855.73	887.5	292.1	11.51	73.2	304.32	.000	0.96	-1.12
33	912.5	292.6	13.45	85.2	302.78	879.12	912.5	293.5	12.63	75.8	303.52	.000	0.85	-0.82
34	937.5	294.1	14.73	87.4	302.19	908.45	937.5	294.9	13.45	75.9	302.78	.000	0.80	-1.28
35	962.5	295.7	16.60	91.4	301.92	942.28	962.5	296.3	14.73	78.2	302.19	.000	0.58	-1.88
36	987.5	297.5	16.82	85.2	301.55	950.83	987.5	297.9	16.60	82.1	301.92	.000	0.41	-0.02
37	1006.2	298.8	17.05	81.1	301.33	957.37	1006.2	299.1	16.82	78.8	301.55	.000	0.25	-0.23

the order of 200–300 mb per day (e.g., Yanai et al. 1973; Cheng 1989). This means that 200–300 mb per day of boundary-layer mass is carried upward in cumulus towers, while the free-atmospheric environment sinks at a comparable rate. Experiments with numerical cloud models show, however, that the conditional instability present in real soundings can be released by convection within a couple of hours (e.g., Soong and Tao 1980; Dudhia and Moncrieff 1987; Krueger 1988). This means that, in the absence of a forcing mechanism to replenish the instability, only on the order of 20 mb ( $1/12$  of 240 mb) of mass can rise to the tropopause before the GCAPE is exhausted. It follows that, in order to obtain an accurate estimate of the GCAPE, the 800-mb-deep troposphere must be divided into about 40 parcels, each 20 mb deep.

We have applied the PM algorithm described in appendix B to all 157 observation times of GATE Phase III (Thompson et al. 1979). With  $N = 9$ , no GCAPE is detected in any of the soundings. Table 1 shows an example of how parcels are rearranged from the given state to the reference state for observation time 71, with  $N = 37$ . In this case, the parcel nearest the surface in the given state rises to 162 mb in the reference state, and all of the intervening parcels are shifted down by one level. Since the lifted parcel conserves its total mixing ratio (we allow no precipitation), its liquid water content in the reference state is extremely large. Below the 162-mb level, the troposphere is warmed and dried by the “compensating subsidence.”

Figure 2 shows the time variation of the GCAPE determined with 37 and 100 parcels; also shown, for comparison, is the time variation of the cloud work function for the case of no entrainment (Arakawa and Schubert 1974). Increasing the number of parcels from 37 to 100 does not make much difference in the GCAPE. There is a strong positive correlation between the GCAPE and the cloud work function. Note, however, that the numerical values of these quantities are radically different. The reason is, quite simply, that their physical meanings are different. The cloud work function represents the kinetic energy per unit mass that can be realized by a parcel rising in a convective updraft. It is apparent from (1.1) that, in contrast, the GCAPE represents the kinetic energy per unit mass that can be realized by all of the air in the column, including rapid convective updrafts and downdrafts, their relatively lethargic large-scale environment, and the horizontal flows that connect these vertical currents together. This explains why the numerical values of the GCAPE are considerably smaller than those of the cloud work function.

Figure 3 shows the time variations of  $T_R - T$  and  $\bar{w}_R - \bar{w}$ , which are, respectively, the departure of the reference state temperature from that of the given state and the departure of the reference state total mixing ratio (vapor plus liquid) from that of the given state. Significant fluctuations occur, and these are correlated in a straightforward way with the fluctuations of the

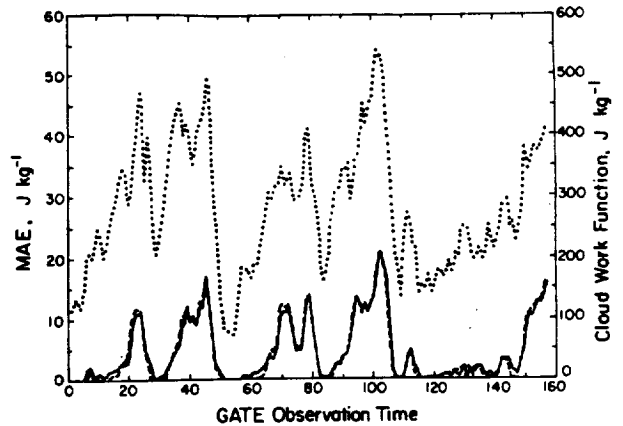


FIG. 2. The time variation of the GCAPE as determined by the PM algorithm with 37 and 100 parcels. Also shown is the time variation of the cloud work function for the case of no entrainment. The cloud work function was determined using nine equally spaced levels; the updrafts were assumed to originate at the lowest level.

GCAPE shown in Fig. 2. The “black spots” seen in the plots, mainly in the upper troposphere, show the locations, in the reference state, of parcels that originate at low levels in the given state (see Table 1).

Figure 4 shows the time averages of  $T_R(p)$ ,  $T(p)$ ,  $\bar{w}_R(p)$ , and  $\bar{w}(p)$  over the 157 GATE observation times. Not surprisingly, the average reference sounding is systematically warmer and drier than the average given sounding, except in the upper troposphere where the lifted parcels are of course much wetter than those they displace.

Figure 5 shows the departures of  $T_R(p)$  and  $T(p)$  from their respective time averages, as well as the departures of  $\bar{w}_R(p)$  and  $\bar{w}(p)$  from their respective time averages. It is clear that *at each pressure level the reference state and the given state tend to vary together*.

Figure 6 makes this point more explicitly by showing the correlations of  $T_R(p)$  with  $T(p)$  and of  $\bar{w}_R(p)$  with  $\bar{w}(p)$  as functions of pressure. To compute these correlations, we included, at each level, all of the observation times for which the GCAPE was found to be positive and the transition from the given state to the reference state involved parcel exchanges at levels up to or beyond the level in question. The figure shows that  $T_R(p)$  and  $T(p)$  are well correlated below about 700 mb and are moderately well correlated up to 200 mb. Similarly,  $\bar{w}_R(p)$  and  $\bar{w}(p)$  are very well correlated up to 300 mb, except near 950 mb, 700 mb, and 450 mb. Large positive correlations indicate that changes in the observed state are systematically “tracking” those of the reference state. As mentioned above, the correlations shown in Fig. 6 are relatively weak near 950 mb, 700 mb, and 450 mb. The 950-mb level is within the boundary layer, and the 700-mb and 450-mb levels are where lifted parcels frequently come to rest in the reference state, as shown in Fig. 3.

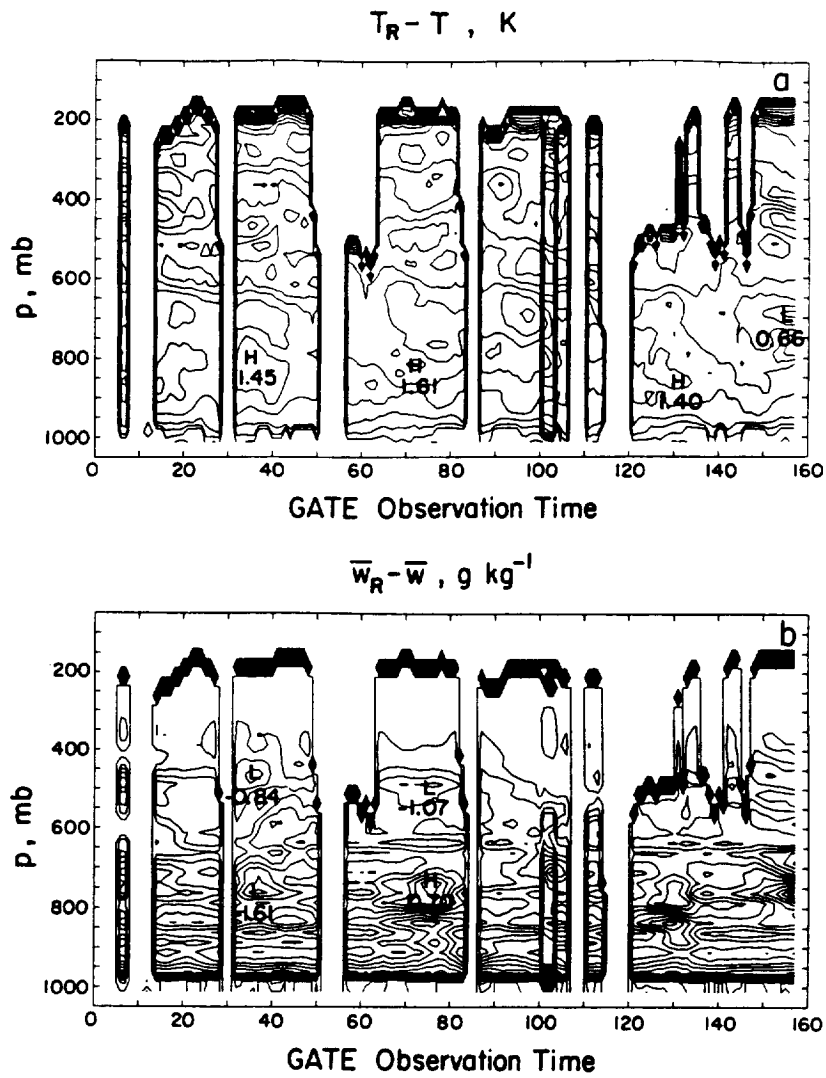


FIG. 3. The time variations of  $T_R - T$  and  $\bar{w}_R - \bar{w}$ , which are, respectively, the departure of the reference state temperature from that of the given state and the departure of the reference state total mixing from that of the given state. The contour interval is 0.25 K for  $T_R - T$  and 0.1  $g\ kg^{-1}$  for  $\bar{w}_R - \bar{w}$ .

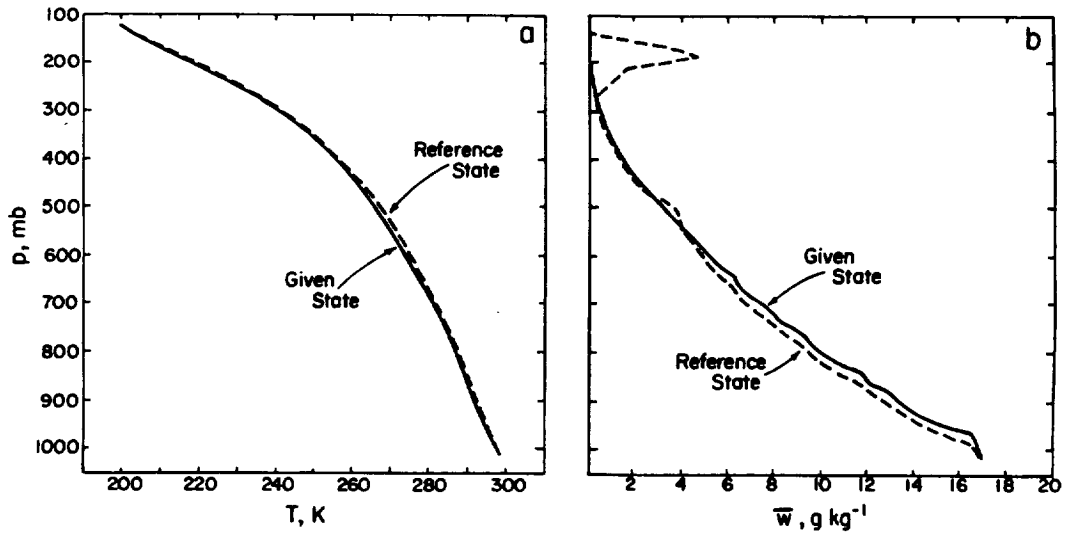


FIG. 4. The time averages of  $T_R(p)$ ,  $T(p)$ ,  $\bar{w}_R(p)$ , and  $\bar{w}(p)$  over the 157 GATE observation times.

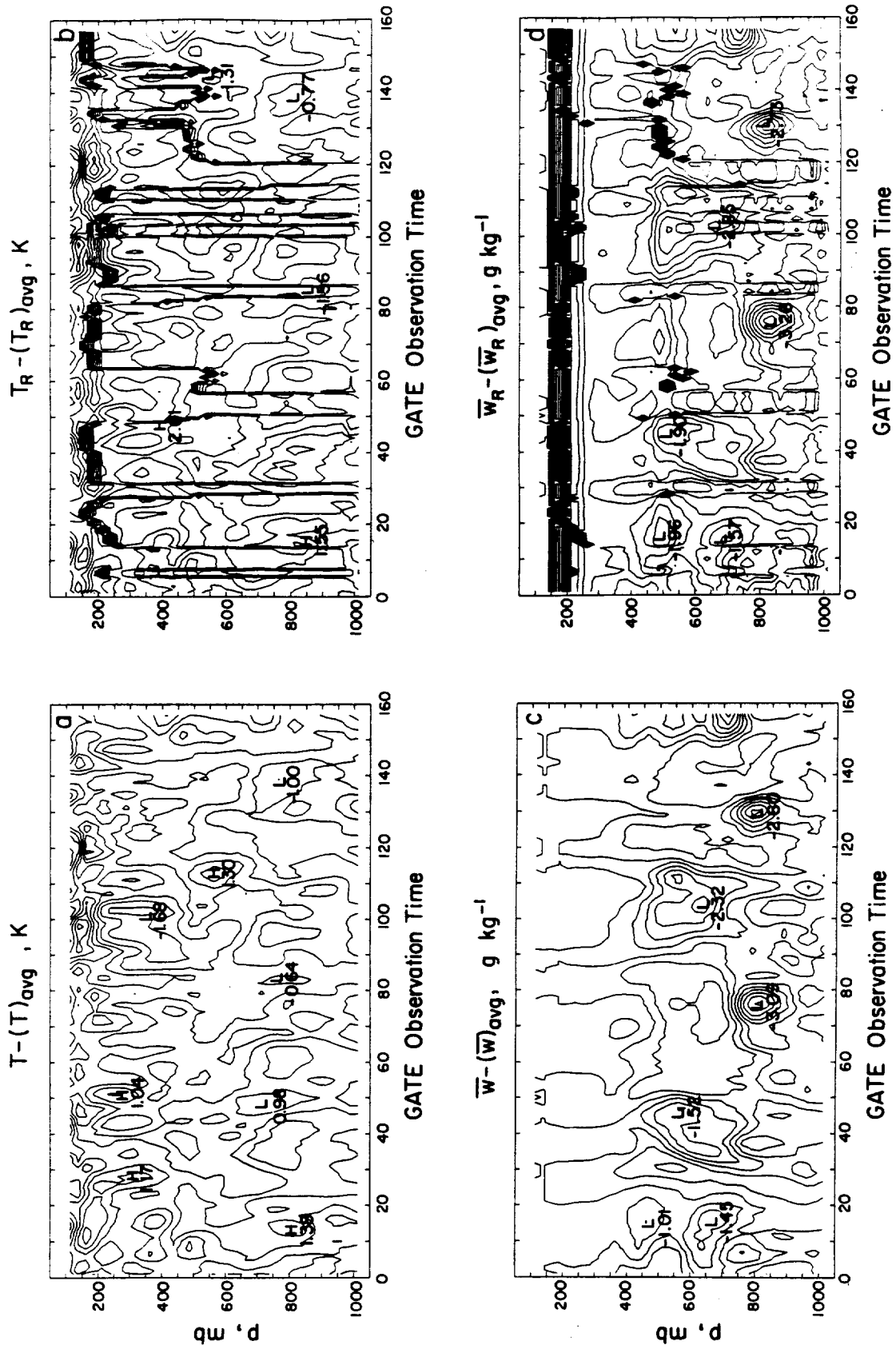


FIG. 5. The departures of  $T_R(p)$  and  $T(p)$  from their respective time averages, and also the departures of  $\bar{w}_R(p)$  and  $\bar{w}(p)$  from their respective time averages. For the temperatures, the contour interval is 0.5 K, and for the mixing ratios it is 0.1  $g\ kg^{-1}$ .

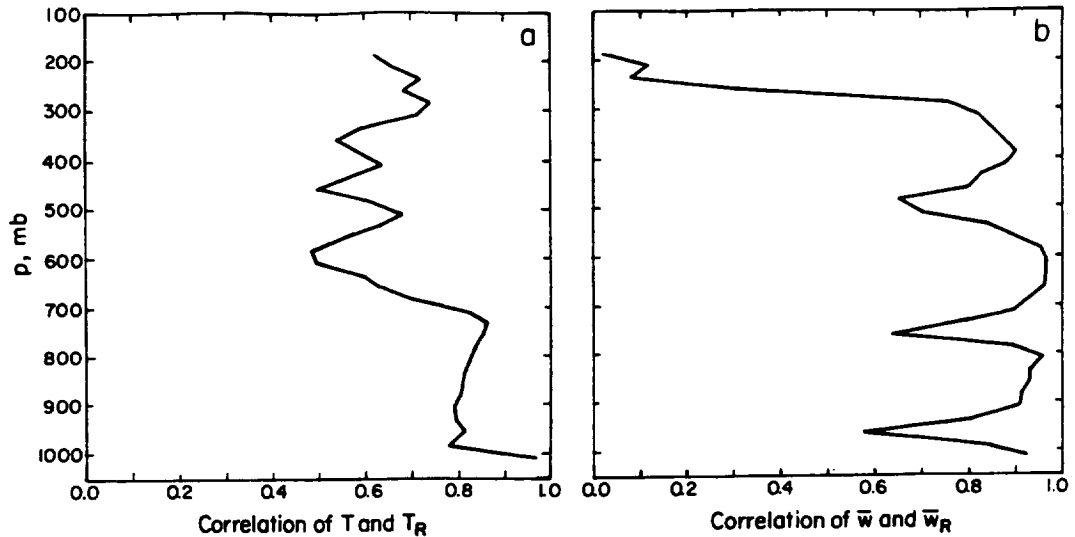


FIG. 6. The temporal correlations of  $T_R(p)$  with  $T(p)$ , and of  $\bar{w}_R(p)$  with  $\bar{w}(p)$ , as functions of pressure.

### 3. A mass flux algorithm to determine the GCAPE

It is somewhat impractical to divide each sounding into scores or hundreds of parcels; an alternative approach is as follows. We divide the given sounding into  $N$  layers, where  $N$  is a manageable number of order 10. Let the mass of layer  $i$  be denoted by  $m_i$ . Imagine that a system of “pipes” is set up, connecting each layer of the sounding with every other layer. Each pipe allows mass to be transferred adiabatically and reversibly in a single direction. Let the amount of mass transferred from layer  $i$  to layer  $j$  be  $M_{i,j}$ . We will use a prime to denote a variable in the reference state. For an intensive variable  $A$  that is conserved under adiabatic reversible processes, we can write

$$m'_i A'_i = m_i A_i + \sum_{j=1}^N M_{j,i} \hat{A}_j - \sum_{j=1}^N M_{i,j} \hat{A}_i, \quad (3.1)$$

where  $\hat{A}$  denotes a “source” value of  $A$  that must be specified. This source value represents a typical value of  $A$  in the layer from which mass is removed. When mass flows from layer  $j$  to layer  $i$ , the source value should be characteristic of layer  $j$ , and vice versa. For this reason, we must require that  $M_{i,j} \geq 0$ .

Three obvious possible choices of  $\hat{A}$  are:

$$\hat{A}_j = A_j, \quad (3.2a)$$

$$\hat{A}_j = A'_j, \quad (3.2b)$$

$$\hat{A}_j = (A_j + A'_j)/2. \quad (3.2c)$$

We shall refer to these as the “forward,” “backward,” and “trapezoidal” schemes, respectively. The trapezoidal scheme has the advantage that it is reversible, which is in accord with our wish to consider reversible adiabatic processes. It also has other advantages as de-

scribed below. We use the trapezoidal scheme in this paper. Putting  $A = 1$  in (3.1) gives a mass conservation equation:

$$m'_i = m_i + \sum_{j=1}^N (M_{j,i} - M_{i,j}). \quad (3.3)$$

We allow only “eddy” mass exchange, so that

$$m'_i = m_i, \quad (3.4)$$

$$\sum_{j=1}^N (M_{j,i} - M_{i,j}) = 0. \quad (3.5)$$

Of course, the diagonal elements  $M_{i,i}$  can be set to zero. Using (3.3)–(3.5), (3.1) can be rewritten as

$$\begin{aligned} \left( m_i + \sum_{j=1}^N \frac{1}{2} M_{j,i} \right) (A'_i - A_i) - \sum_{j=1}^N \frac{1}{2} M_{j,i} (A'_j - A_j) \\ = \sum_{j=1}^N M_{j,i} (A_j - A_i). \end{aligned} \quad (3.6)$$

These equations can be used to evaluate the GCAPE of conditionally unstable soundings. If a set of  $M_{i,j}$  is specified, (3.6) can be applied to determine the changes in the entropy and total mixing ratio of the air. The total enthalpy of the new state can then be evaluated and compared with that of the given state. We seek the matrix  $M_{i,j}$  such that the total enthalpy of the final state is minimized, subject to the constraint (3.5). Of course, we must also restrict ourselves to nonnegative  $M$ 's.

With this mass flux method, as with the parcel-moving method, a conditionally unstable given state corresponds to a reference state in which some portion of the air must be saturated. As a result, the amount of

mass lifted from lower levels to upper levels may have to attain a finite minimum value before any decrease in the total enthalpy occurs. It should also be noted that (3.6) only determines the *average* entropy and total mixing ratio of the adjusted state; the adjusted enthalpy has to be based on these average values.

As an example, consider the simple case  $N = 2$ . Then (3.5) implies that

$$M_{1,2} = M_{2,1} = M. \quad (3.7)$$

After some manipulation, we find from (3.6) that

$$A'_1 - A_1 = \frac{m_2 M (A_2 - A_1)}{m_1 m_2 + \frac{1}{2} M (m_1 + m_2)}, \quad (3.8)$$

$$A'_2 - A_2 = \frac{-m_1 M (A_2 - A_1)}{m_1 m_2 + \frac{1}{2} M (m_1 + m_2)}. \quad (3.9)$$

For  $M \rightarrow \infty$ , and if  $m_1 = m_2$ , (3.8) and (3.9) imply that the parcels exchange places: parcel number 1 takes property  $A_2$ , and vice versa. The trapezoidal scheme thus gives us a parcel swapper in the limit of large  $M$ . This is an attractive property of the scheme.

We have applied these equations to the idealized two-level "sounding" given in Table 2;  $\theta$  is the potential temperature,  $\theta_e$  is equivalent potential temperature, and  $\theta_{es}$  is saturation equivalent potential temperature. The two layers are assumed to be of equal thickness, with surface pressure 1000 mb and top pressure 100 mb. Both levels are nearly saturated. The relative humidity at 775 mb is so high that even slight lifting is sufficient to produce condensation. Since the  $\theta_e$  of the lower layer exceeds the  $\theta_{es}$  of the upper layer, the sounding is conditionally unstable. Following L79, we assume that entropy and total mixing ratio are conserved. We tried various values of  $M/m_2$ , increasing from zero by steps of 0.01. The results are shown in Fig. 7. The upper level becomes saturated with even a one percent injection of air from the lower level. A minimum of the total enthalpy occurs for  $M/m_2 = 0.11$ ; this corresponds to the reference state. The GCAPE per unit mass is  $13.1 \text{ J kg}^{-1}$ . In the limit  $M/m_2 \rightarrow \infty$ , the change in  $H$  approaches  $1397 \text{ J kg}^{-1}$ . Clearly, for this particular case the behavior of the algorithm as  $M \rightarrow \infty$  is irrelevant.

#### 4. Penetrators

For  $N > 2$ , we need a way to ensure that (3.5) is automatically satisfied. This is done by introducing

TABLE 2. A hypothetical two-level sounding used to generate the results shown in Fig. 7.

$p$ (mb)	$T$ (K)	$\theta$ (K)	$q$ (g kg <sup>-1</sup> )	$\theta_e$ (K)	$\theta_{es}$ (K)
325	250	344.78	1.78	350.86	351.04
775	290	311.93	15.70	354.71	354.89

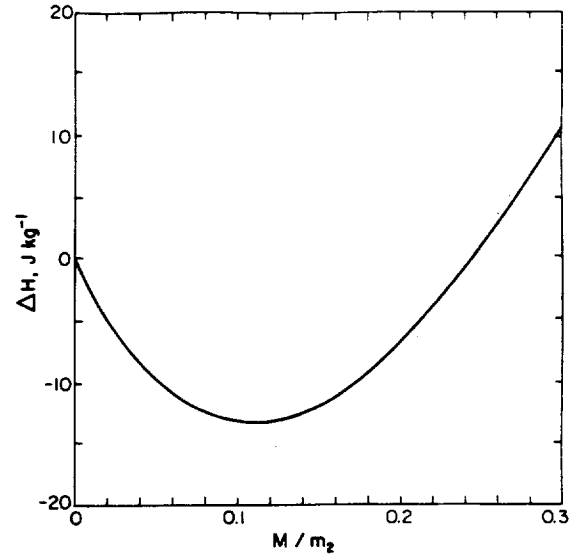


FIG. 7. Departure of the total enthalpy from that of the given state, plotted as a function of  $M/m_2$ , for the two-level "sounding" given in Table 2. Here  $M$  is the amount of mass exchanged between the layers, and  $m_2$  is the mass of the lower layer.

"penetrators." A penetrator  $P_{i,j}$  consists of a mass flux that penetrates from layer  $i$  to layer  $j$ , with a compensating, *nonpenetrative, level-by-level return flow*. Each penetrator satisfies (3.5), so any superposition of penetrators also satisfies (3.5). By analogy with (3.1), the change in  $A_i$  due to an ensemble of penetrators is given by

$$\begin{aligned} m'_i A'_i - m_i A_i &= \sum_{j=1}^N P_{j,i} (\hat{A}_j - \hat{A}_i) \\ &- \sum_{j=1}^N P_{i,j} \hat{A}_i + \sum_{j<i} P_{i,j} \hat{A}_{i-1} + \sum_{j>i} P_{i,j} \hat{A}_{i+1} \\ &+ \sum_{j<i} \sum_{l>i} P_{j,l} (\hat{A}_{i+1} - \hat{A}_i) + \sum_{j>i} \sum_{l<i} P_{j,l} (\hat{A}_{i-1} - \hat{A}_i). \end{aligned} \quad (4.1)$$

On the right-hand side of (4.1), the terms on the first line represent the effects of "incoming" penetrators that terminate at level  $i$ , those on the second line represent the effects of "outgoing" penetrators that originate at level  $i$ , and the terms on the third line represent the effects of penetrators that are "just passing through" level  $i$ . Putting  $A = 1$ , and using

$$P_{i,i} = 0 \quad (4.2)$$

for all  $i$ , we find that (4.1) reduces to

$$m'_i - m_i = 0; \quad (4.3)$$

this is identical to (3.4), and it follows immediately that (3.5) is automatically satisfied by any combination of penetrators as intended.

We assume that any combination of mass fluxes satisfying (3.5) is equivalent to a suitably chosen combination of penetrators. After some algebraic manipulation, (4.1) can be rewritten as

$$m_i(A'_i - A_i) = \sum_{j-i > 1} P_{j,i}(\hat{A}_j - \hat{A}_i) + (\hat{A}_{i-1} - \hat{A}_i)(Q_{i,i-1} + \sum_{j < i-1} P_{i,j} + \sum_{j > i} \sum_{l < i} P_{j,l}) + (\hat{A}_{i+1} - \hat{A}_i)(Q_{i,i+1} + \sum_{j > i+1} P_{i,j} + \sum_{j < i} \sum_{l > i} P_{j,l}), \quad (4.4)$$

where

$$Q_{i,i-1} = P_{i,i-1} + P_{i-1,i}. \quad (4.5)$$

Notice that  $P_{i,i-1}$  and  $P_{i,i+1}$  do not appear explicitly in (4.4), although they do appear implicitly through  $Q_{i,i-1}$  and  $Q_{i,i+1}$ . The interpretation is straightforward. A penetrator that joins two neighboring layers does not really penetrate at all. As a result, the injection of air from  $i$  to  $i+1$  with the accompanying return flow from  $i+1$  to  $i$  has exactly the same effect as injection from  $i+1$  to  $i$  with a return flow from  $i$  to  $i+1$ . This means that  $P_{i+1,i}$  and  $P_{i,i+1}$  are redundant; they do the same thing. That is why only their sum,  $Q_{i,i+1}$ , appears in (4.4).

To determine the reference state and the GCAPE, we must find the values of the  $P$  and  $Q$  such that the total enthalpy of the adjusted state is minimized. These solutions are subject to the requirement that the  $P$  and  $Q$  must be nonnegative, since their source regions have been specified. For an  $N$ -layer sounding, we can define  $N^2$  different values of  $P$ . Not all of these are meaningful, however. As indicated in (4.2), the diagonal elements of the  $P$  matrix can be set to zero, since they have no effect on the sounding. In addition, the redundancy of the neighboring-layer  $P$ , discussed above, allows us to replace  $2(N-1)$  of the  $P$  by  $(N-1)Q$ , effectively reducing the number of unknowns by  $N-1$ . The actual number of unknowns is then  $N^2 - N - (N-1) = (N-1)^2$ . In general, there are  $(N-1)Q$  and  $(N-2)(N-1)P$ . Table 3 shows how the numbers of the various unknowns change as  $N$  changes. Given the results of section 2, we can anticipate that, in most

cases of practical interest, many of these unknowns will turn out to be zero. Unfortunately, there is no obvious way to know in advance which ones these will be.

### 5. Application of penetrators to the GATE data

For selected GATE observation times, and allowing only 9 layers, we have considered each possible  $P$  and each possible  $Q$ , one at a time, and computed the greatest possible reduction in total enthalpy and the corresponding fraction of mass transported out of the layer from which the penetrator originates. For GATE observation time 102, Fig. 8 illustrates the change in the total enthalpy as a function of  $P_{i,j}/m_i$  for four different choices of  $i$  and  $j$ . The results are plotted for  $0 \leq P_{i,j}/m_i \leq 1$ , although in principle arbitrarily large positive values could be considered. In the first case, the enthalpy increases monotonically, so that no GCAPE can be realized. In the second case, a single well-defined minimum of the total enthalpy occurs for  $P_{i,j}/m_i = 0.55$ ; this is similar to Fig. 7. In the third case, the enthalpy decreases monotonically out to  $P_{i,j}/m_i = 1.0$ , suggesting that  $\Delta H$  is minimized in the limit as  $P_{i,j}/m_i \rightarrow \infty$ . In the fourth case, a broad, flat minimum of the total enthalpy occurs for  $0.2 < P_{i,j}/m_i < 0.6$ .

These four cases illustrate all of the behaviors that we have found in the GATE data. Cases for which multiple, distinct enthalpy minima occur for distinct values of the penetrator mass flux were not encountered. We have not proven that such cases cannot occur, however.

Table 4 shows the maximum total enthalpy reduction that can be produced by each penetrator for several GATE observation times, and Table 5 shows the corresponding values of  $P_{i,j}/m_i$ . These results are for  $N = 9$ . Recall that the parcel-moving algorithm did not detect any GCAPE with  $N = 9$ . Clearly the penetrator algorithm has succeeded in detecting the GCAPE that is present in the soundings. As discussed earlier, zeroes are guaranteed to occur, in both tables, along the diagonals that run from top left to bottom right, since these trivial "penetrators" have no effect on the soundings. Entries below the diagonals represent penetrators

TABLE 3. The numbers of  $P$  and  $Q$  and the total number of unknowns as a function of the number of model layers.

Number of layers	Number of $P$	Number of $Q$	Total number of unknowns
2	0	1	1
3	2	2	4
4	6	3	9
5	12	4	16
6	20	5	25
7	30	6	36
8	42	7	49
9	56	8	64
10	72	9	81

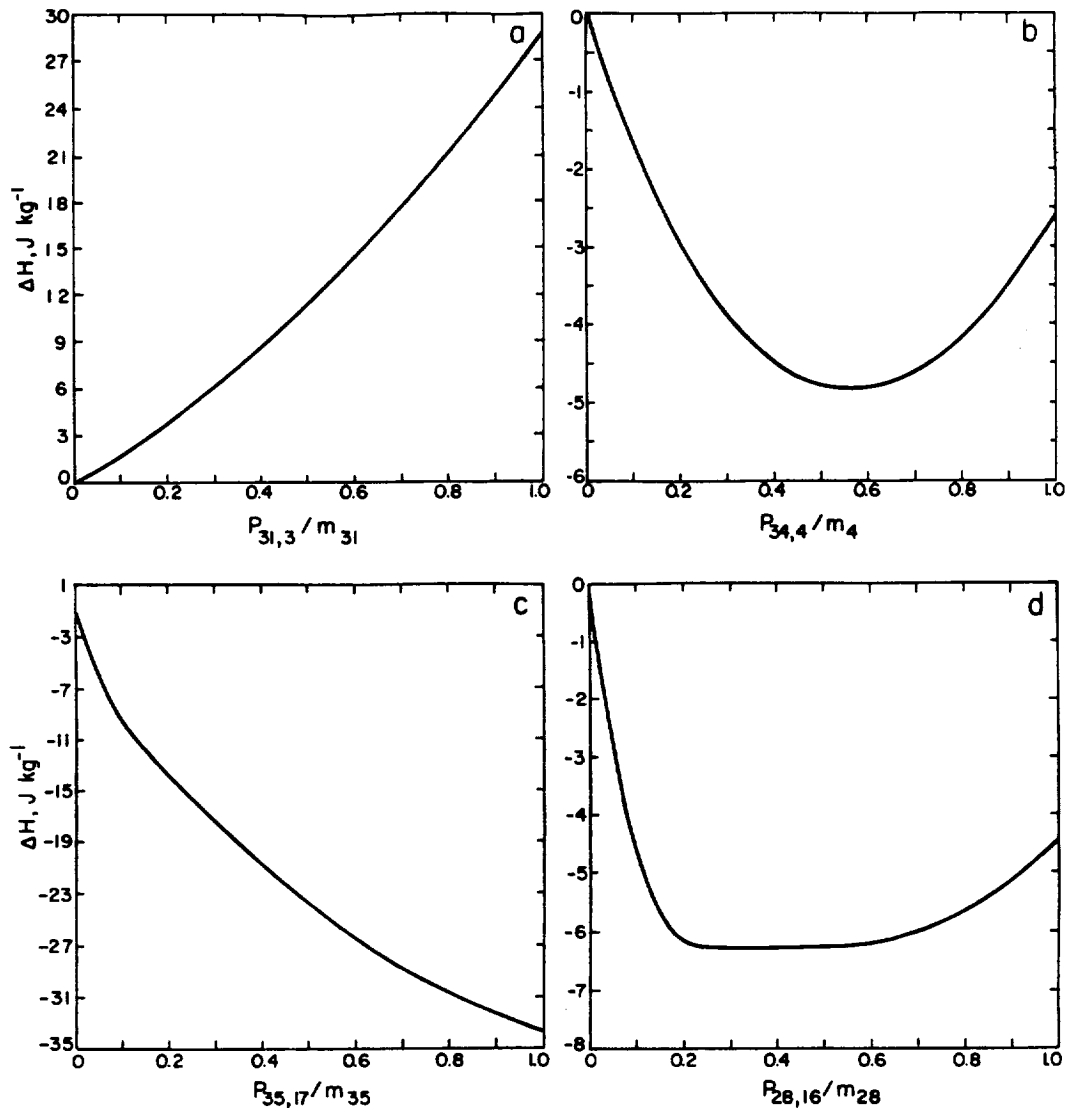


FIG. 8. The change in the total enthalpy as a function of  $P_{i,j}/m_i$ , for: (a)  $i = 31$  and  $j = 3$  (penetrator originating at 862 mb and terminating at 162 mb); (b)  $i = 34$  and  $j = 4$  (penetrator originating at 937 mb and terminating at 187 mb); (c)  $i = 35$  and  $j = 17$  (penetrator originating at 962 mb and terminating at 512 mb); and (d)  $i = 28$  and  $j = 16$  (penetrator originating at 787 mb and terminating at 487 mb). The GATE observation time is 102.

that penetrate upward, with a compensating downward layer-by-layer return flow; and entries above the diagonal represent penetrators that penetrate downward, with a compensating upward layer-by-layer return flow. The entries nearest the diagonals represent  $Q$ , and (4.5) guarantees that they are symmetric, i.e.,  $Q_{i,i-1} = Q_{i-1,i}$ . We naturally expect upward penetrators to dominate, and they do, with the largest number of nonzero entries and the largest enthalpy reductions, particularly for penetrators originating near the lower boundary and penetrating to the upper troposphere.

Surprisingly, however, our results show that it is possible for downward penetrators to release GCAPE in some cases. For example, at GATE observation time 45, a penetrator originating at 447 mb can release

GCAPE by penetrating downward to 782 mb or below. In such cases, the compensating layer-by-layer upward motion produces condensation, and this accounts for the release of available energy. Although it may well be dynamically impossible for such penetrators to develop, this issue deserves further study.

How can we determine the set of  $P$  and  $Q$  that is required to reach the reference state for the case of arbitrary  $N$ ? For  $N = 2$ , discussed in section 3, we searched a one-dimensional space by brute force to find the value of the single unknown, which we now recognize as a  $Q$ . A glance at Table 3 shows that this approach quickly becomes impractical for arbitrary  $N$ .

As an alternative, we could use a numerical method to determine the partial derivative  $H$  with respect to

TABLE 4. The maximum enthalpy reduction produced by each penetrator for several GATE observation times using nine layers. Zeroes are omitted from the tables. The row indicates the pressure from which the penetrator originates, while the column indicates the pressure to which the penetrator penetrates.

	112.5	224.2	335.9	447.6	559.3	671.0	782.7	894.4	1006.1
GATE observation time 4									
112.5									
224.2									
335.9					1.03				
447.6				1.03					0.06
559.3							7.36	5.59	9.23
671.0				0.36		7.36		0.32	4.48
782.7				1.14		6.80	0.32		7.49
894.4				8.80	7.61	18.81	7.61	7.49	
1006.1		1.28	3.78						
GATE observation time 45									
112.5									
224.2									
335.9							0.68	5.23	4.26
447.6						3.77	9.74	21.59	19.73
559.3				0.29	3.77		9.05	24.39	23.87
671.0				7.81	15.76	9.05		12.58	13.17
782.7				28.20	38.70	27.48	12.58		2.29
894.4		0.01	4.17	61.30	65.22	45.16	19.62	2.29	
1006.1		20.61	33.23						
GATE observation time 69									
112.5									
224.2									
335.9					4.30	0.70			0.04
447.6					14.36	5.53	0.03	1.67	2.35
559.3			6.33	14.36				0.02	0.68
671.0			7.66	12.06				0.06	1.62
782.7			2.36	2.40				7.98	17.33
894.4			6.36	7.36		0.01	7.98		13.01
1006.1		25.26	33.42	29.42	13.91	13.95	27.15	13.01	
GATE observation time 85									
112.5									
224.2									
335.9									
447.6									
559.3								0.25	2.19
671.0								3.16	8.54
782.7						0.40	3.16		6.74
894.4						9.84	12.75	6.74	
1006.1		1.60	5.07	5.47	6.68				
GATE observation time 102									
112.5									
224.2									
335.9							2.76	8.10	5.37
447.6						1.71	19.68	30.72	24.94
559.3							24.86	36.93	31.94
671.0					1.71			9.15	8.81
782.7				1	25.46	24.86			2.20
894.4		0.72	6.93	29.29	45.89	37.82	9.15		
1006.1		28.40	0.80	63.85	72.64	52.96	15.21	2.20	

each of the  $P$  and  $Q$ . The results could be arranged as a matrix. We could then try a linearization approximation in which this matrix is used to find the values

of the  $P$  and  $Q$  that minimize  $H$ . Unfortunately, this approach fails, for two reasons. First, it cannot guarantee that the  $P$  and  $Q$  are nonnegative. Second, as is

TABLE 5. The values of  $P_{i,j}/m_i$  associated with the maximum enthalpy reduction by each penetrator for several GATE observation times using nine layers. Zeroes are omitted from the tables. The row indicates the pressure from which the penetrator originates, while the column indicates the pressure to which the penetrator penetrates.

	112.5	224.2	335.9	447.6	559.3	671.0	782.7	894.4	1006.1
GATE observation time 4									
112.5									
224.2									
335.9									
447.6					0.07				
559.3				0.07					0.01
671.0							0.24	0.17	0.19
782.7				0.02		0.24		0.06	0.18
894.4				0.04		0.17	0.06		0.36
1006.1		0.08	0.14	0.21	0.30	0.39	0.28	0.36	
GATE observation time 45									
112.5									
224.2									
335.9									
447.6							0.04	0.11	0.10
559.3						0.15	0.20	0.27	0.26
671.0				0.02	0.15		0.30	0.37	0.35
782.7				0.11	0.22	0.30		0.36	0.32
894.4		0.01	0.18	0.44	0.56	0.56	0.36		0.22
1006.1		0.34	0.51	0.73	0.84	0.81	0.55	0.22	
GATE observation time 69									
112.5									
224.2									
335.9					0.10	0.04			0.01
447.6					0.23	0.13	0.01	0.06	0.07
559.3			0.08	0.23				0.01	0.04
671.0			0.07	0.16				0.02	0.09
782.7			0.03	0.06				0.27	0.36
894.4			0.05	0.09		0.01	0.27		0.55
1006.1		0.34	0.41	0.39	0.37	0.43	0.55	0.55	
GATE observation time 85									
112.5									
224.2									
335.9									
447.6									
559.3									
671.0								0.04	0.10
782.7								0.19	0.25
894.4						0.04	0.19		0.35
1006.1		0.09	0.16	0.20	0.26	0.36	0.39	0.35	
GATE observation time 102									
112.5									
224.2									
335.9									
447.6							0.09	0.15	0.12
559.3						0.10	0.29	0.33	0.30
671.0					0.10		0.45	0.43	0.39
782.7				0.12	0.28	0.45		0.31	0.26
894.4		0.06	0.26	0.47	0.60	0.55	0.31		0.23
1006.1		0.43	0.56	0.75	0.86	0.80	0.46	0.23	

clear from Figs. 7 and 8,  $H$  varies nonlinearly with the  $P$  and  $Q$ . This nonlinearity arises from the nonlinear dependence of the enthalpy of saturated air on the en-

trophy and total mixing ratio. The nonlinearity is actually critical for the existence of an isolated *minimum* value of  $H$  for finite positive values of the  $P$  and  $Q$ .

To see this, consider the *dry* statically unstable case with  $N = 2$ , as discussed in the Introduction. If the trapezoidal algorithm is used, we find that there is no minimum of  $H$  for finite  $Q$ . Instead,  $H$  decreases monotonically as  $Q$  increases and is minimized when  $Q \rightarrow \infty$ , i.e., when the parcels are swapped.

The nonlinearity also rules out the use of linear programming methods, which, if they were applicable, could ensure nonnegativity of the  $P$  and  $Q$ . It appears that we must employ nonlinear programming, which is relatively unknown territory with few strong theorems. This problem is left to the future.

## 6. Summary and concluding discussion

We have demonstrated that the concept of moist available energy, as formulated by Lorenz (1978, 1979), can be used to define a generalized convective available kinetic energy. An advantage of this GCAPE is that it can be determined without arbitrary assumptions about the level of origination of the convective updrafts. It can also include, without modification, the effects of evaporatively cooled convective downdrafts originating from elevated cloud layers, as well as the energetic consequences of compensating vertical motions in the environment of the concentrated vertical currents.

Using GATE data, we have demonstrated that the GCAPE is highly correlated with conventional measures of conditional instability. It has also been shown that changes of the reference state are highly correlated with changes of the observed GATE soundings. This suggests that the tropical atmosphere is forced to remain close to the reference state. The agency responsible for enforcing this is, presumably, cumulus convection.

This paper raises a number of questions that are left for the future. For example:

- For each observation time, what mass exchanges are required to reach the reference state? To answer this question, the nonlinear optimization problem discussed at the end of section 5 must be solved.
- What time changes of the GCAPE and the reference state would occur if the observed large-scale circulations acted alone, without compensating cumulus effects? How do these hypothetical changes in the GCAPE compare to those that actually occur?
- As discussed by L78, the global reference state used in the definition of the MAE is, in general, horizontally inhomogeneous; both saturated and unsaturated air can occur on each pressure surface. In the context of GCAPE, is it useful to allow the reference state to be horizontally inhomogeneous? As noted in sections 3 and 4, in applying the penetrator algorithm we have assumed that the enthalpy of each grid cell can be obtained from the average entropy and moisture content of the cell. In reality, a cell may contain both saturated

and unsaturated volumes, e.g., if it has received an injection of cloudy air from a lower level. These two volumes will generally have distinct entropies and total mixing ratios. Since the enthalpy is a nonlinear function of the entropy and the total mixing ratio, the average enthalpy of the cell is not the same as the enthalpy based on the average entropy and the average total mixing ratio. This means that the fraction of each cell that is occupied by cloudy air will influence the total enthalpy of the cell and, therefore, the total enthalpy of the air column. It also means, interestingly, that the reference state corresponds to a certain cloud amount at each level.

- How do the results change if the penetrators are endowed with various properties? For example, we might choose to give up the assumption of adiabatic reversible mass transfer and allow a process in which some of the water vapor that is condensed inside penetrators precipitates out. This irreversible process would avoid the unrealistically large liquid water concentrations that appear in the "exact" reference state. One way of thinking about this possibility is that the physical system *tries* to attain the reference state but cannot actually do so because irreversibility inevitably creeps in.

- Besides the absolute minimum of  $H$  that denotes the reference state, do local, relative minima ever occur in the mass-exchange space? Imagine a plot like panel b of Fig. 8, but with two well-separated minima, one of which is deeper than the other. Can such a thing happen?

The penetrator algorithm discussed in section 5 bears a strong resemblance to the mass-flux methods that have been developed for use in cumulus parameterizations (e.g., Arakawa and Schubert 1974). It is interesting that such methods arise naturally in an attempt to evaluate the GCAPE. Our results encourage us to believe that it may be possible to develop a cumulus parameterization based on the concept of GCAPE and the associated reference state. Several existing cumulus parameterizations are based on the concept of adjustment towards an equilibrium sounding (Manabe 1965; Arakawa and Schubert 1974; Betts and Miller 1986; also see Arakawa and Chen 1987). The trick, of course, is to identify the equilibrium sounding. Existing parameterizations do so using simple cloud models (Arakawa and Schubert 1974) or empirical assumptions (Betts and Miller 1986).

In some parameterizations (Manabe 1965; Arakawa and Schubert 1974), but not all (Betts and Miller 1986), the equilibrium state is assumed to be one in which little or no buoyancy can be realized by a lifted parcel; in the present context this would correspond to a sounding with no GCAPE, i.e., the reference state. There is considerable empirical evidence that the convective atmosphere is prevented from attaining a high degree of conditional instability (e.g., Lord and Ar-

akawa 1982; Xu and Emanuel 1989). It is natural to suppose that Lorenz's reference state represents a suitable equilibrium sounding towards which a cumulus parameterization might "adjust."

The results presented in section 2 provide evidence for this idea. In particular, we note the "closeness" of the observed GATE soundings to the corresponding reference soundings and, more importantly, the strong temporal correlation between the reference state and the given state, as revealed by Figs. 5 and 6. This correlation suggests that these two states are coupled together by a very efficient and "fast" physical process, which, we assert, is cumulus convection.

The appeal of this concept is that Lorenz's reference state can be found from first principles without cloud models or empirical assumptions. This suggests that a cumulus parameterization based on the concept of GCAPE might be relatively simple and relatively free from questionable modeling assumptions.

*Acknowledgments.* Dr. Kuan-Man Xu's thorough and constructive review led to substantial improvements in the final version of this paper. We are indebted to Professor Richard Reed for allowing us to use the GATE data as analyzed by his group. Support has been provided by the National Science Foundation under Grant ATM-8907414 to Colorado State University. Computing resources were provided by the National Center for Atmospheric Research.

#### APPENDIX A

##### Thermodynamic Formulas

The purpose of this appendix is to summarize the thermodynamic formulas that were actually used. Further details, including derivations of some of the equations, can be found in L79.

As input, the temperature and total mixing ratio of water were read as functions of pressure. We thus have a list of parcels, each of which resides in the given state at a certain pressure with a certain temperature and a certain mixing ratio. For simplicity, the pressures are equally spaced.

Next, the entropy and enthalpy of each parcel are determined, using

$$(1 + \bar{w})_s = (c_p + \bar{w}c_{pw}) \ln T - R \ln(p - e) - \bar{w}R_w \ln e - (\bar{w} - w)L/T, \quad (\text{A.1})$$

$$(1 + \bar{w})h = (c_p + \bar{w}c_{pw})T - (\bar{w} - w)L, \quad (\text{A.2})$$

where  $\bar{w}$  is the total mixing ratio of water (liquid plus vapor),  $s$  is the entropy per unit mass,  $c_p$  is the specific heat at constant pressure of dry air,  $c_{pw}$  is the specific heat at constant pressure of water vapor,  $T$  is the temperature,  $R$  is the gas constant for dry air,  $p$  is the pressure,  $e$  is the partial pressure of water vapor,  $R_w$  is the specific gas constant for water vapor,  $w$  is the mixing ratio of water vapor,  $L$  is the latent heat of condensa-

tion, and  $h$  is the enthalpy per unit mass. Note that (A.1)–(A.2) are identical to (15)–(16) of L79, except that (15) of L79 contains a typographical error. [In the first term of the second line of L79's Eq. (15),  $w$  is written in place of  $\bar{w}$ .] An explanation of (A.1)–(A.2) is given by L79. Since  $T$ ,  $p$ , and  $\bar{w}$  are known, evaluation of  $w$ ,  $L(T)$ , and  $e$  is straightforward. At the same time, the parcel's saturation temperature and pressure are determined (Betts 1982).

When a parcel is displaced, it strictly conserves its entropy and total mixing ratio, as well as its saturation temperature and pressure. When it arrives at a new pressure, its new enthalpy can be determined as follows. If it is placed at a pressure greater than its saturation pressure, then it is unsaturated, so that  $\bar{w} = w$ , and  $e$  can be determined from

$$e = \frac{wp}{\epsilon + w}, \quad (\text{A.3})$$

where  $\epsilon = R/R_w$ . If it is displaced to a pressure less than its saturation pressure, then  $\bar{w} > w$ , and  $T$ ,  $w$ , and  $e$  must be determined iteratively. As a first guess, assume that  $T$  is equal to the saturation temperature. This assumed temperature can be used to evaluate  $e$  and  $w$ . Then (A.1) is used to find a provisional value of the entropy, here denoted by  $\hat{s}$  and also  $(\partial s/\partial T)_p$ . A correction to the temperature is then obtained from

$$\Delta T = \frac{s - \hat{s}}{(\partial s/\partial T)_p}. \quad (\text{A.4})$$

The iteration is repeated until  $\Delta T$  is sufficiently small, at which point  $T$ ,  $w$ , and  $e$  have been determined with sufficient accuracy. Then the enthalpy is evaluated from (A.2).

Finally, the virtual temperature must be determined. This is obtained from

$$T_v = T \left( \frac{1 + w/\epsilon}{1 + \bar{w}} \right). \quad (\text{A.5})$$

Recently we have generalized our thermodynamic equations to allow for the effects of ice, following the approach of Ooyama (1990). Discussion of this straightforward change will be given elsewhere.

#### APPENDIX B

##### A Parcel-moving Algorithm

The parcel-moving algorithm described here is a modified version of that given by L79. Our goal is to find the pressure at which each parcel resides in the reference state. We begin by determining which parcel resides at the lowest pressure in the reference state, then consider the second-lowest pressure, and so on, until all parcels have been assigned reference-state pressures. Lorenz's parcel-moving algorithm is based on the simple fact that the virtual potential temperature cannot decrease upward in the reference state.

TABLE 6. Reference sounding determined with the test suggested by Lorenz for GATE observation time 71. Here RH denotes the relative humidity. The corresponding correct results are given in Table 1.

Level	$p$ (mb)	$T$ (K)	$\bar{w}$ (g kg <sup>-1</sup> )	RH (%)	$\theta_p$ (K)	$\bar{w} - w$ (g kg <sup>-1</sup> )	$T_R - T$ (K)	$\bar{w}_R - \bar{w}$ (g kg <sup>-1</sup> )
1	112.5	197.3	0.008	67.7	368.3	0.00	0.0	0.0
2	137.5	201.6	0.008	41.3	355.2	0.00	0.0	0.0
3	162.5	207.3	0.014	40.1	348.3	0.00	0.0	0.0
4	187.5	218.8	17.05	13 221.0	347.1	16.92	5.5	17.0
5	212.5	225.7	16.82	6 716.4	345.6	16.57	6.0	16.8
6	237.5	228.2	0.028	9.5	344.1	0.00	2.4	-0.1
7	262.5	237.6	16.60	2 356.5	342.8	15.90	5.9	16.5
8	287.5	239.5	0.051	6.6	342.0	0.00	2.4	-0.2
9	312.5	244.3	0.096	8.5	340.6	0.00	2.2	-0.2
10	337.5	248.9	0.130	8.2	339.4	0.00	2.5	-0.2
11	362.5	253.4	0.223	10.1	338.6	0.00	3.1	-0.2
12	387.5	257.5	0.285	9.8	337.6	0.00	3.5	-0.3
13	412.5	260.9	0.335	9.2	336.1	0.00	3.6	-0.6
14	437.5	264.1	0.422	9.5	334.5	0.00	3.7	-0.9
15	462.5	267.1	0.612	11.7	333.0	0.00	4.8	-1.4
16	487.5	269.9	0.931	5.0	331.5	0.00	4.9	-2.0
17	512.5	272.4	1.338	18.8	323.0	0.00	5.4	-2.4
18	537.5	274.5	1.972	25.1	328.1	0.00	5.5	-2.6
19	562.5	276.1	2.946	34.9	326.0	0.00	5.4	-2.3
20	587.5	277.7	3.774	41.7	323.9	0.00	5.1	-2.0
21	612.5	279.2	4.578	47.4	322.0	0.00	4.6	-1.8
22	637.5	280.6	5.225	51.1	320.0	0.00	4.0	-2.0
23	662.5	282.0	5.806	53.4	318.3	0.00	3.6	-1.8
24	687.5	283.8	6.329	53.6	317.0	0.00	3.5	-1.9
25	712.5	285.5	7.209	56.4	315.9	0.00	3.5	-1.6
26	737.5	287.1	7.584	55.3	314.6	0.00	3.5	-1.1
27	762.5	288.7	8.204	55.7	313.5	0.00	3.5	-0.5
28	787.5	290.2	8.766	55.9	312.3	0.00	3.7	-0.3
29	812.5	291.6	8.719	52.5	311.0	0.00	4.1	-0.5
30	837.5	292.9	8.730	49.6	309.8	0.00	4.4	-1.9
31	862.5	294.0	8.456	46.3	308.2	0.00	4.3	-3.1
32	887.5	294.8	9.172	49.1	306.7	0.00	3.7	-3.5
33	912.5	295.7	10.67	55.6	305.5	0.00	3.1	-2.8
34	937.5	296.7	11.51	57.9	304.3	0.00	2.6	-3.2
35	962.5	298.0	12.63	60.5	303.5	0.00	2.3	-4.0
36	987.5	299.3	13.45	61.0	302.8	0.00	1.8	-3.4
37	1006.2	300.1	14.73	64.9	302.2	0.00	1.3	-2.3

Although this fact is intuitively obvious, its proof, based on the thermodynamic relations given in appendix A, is worth outlining. The first law of thermodynamics can be written in the form

$$dh = Tds + \alpha dp. \quad (\text{B.1})$$

A parcel that is adiabatically displaced to a lower pressure (i.e., with  $ds = 0$ ) thus experiences a decrease in its enthalpy proportional to the product of the pressure decrease and its specific volume.

Using the methods of appendix A, the virtual temperature of a parcel can be determined as a function of its entropy, total mixing ratio, and pressure. The sounding consists of a set of parcels with certain entropies and total mixing ratios. Each parcel is assigned to a certain pressure level. Let  $p_A$  be the lowest pressure in the sounding (the "top" pressure level), and let  $p_B$  be the highest pressure in the sounding (the "bottom" pressure level). Let the virtual temperatures obtained

for parcel  $k$  at pressures  $p_A$  and  $p_B$  be denoted  $T_{vA}(k)$  and  $T_{vB}(k)$ , respectively. As discussed by L79, the parcel that resides at  $p_A$  in the reference state must be either the one with the highest  $T_{vA}(k)$  or the one with the highest  $T_{vB}(k)$ .

To decide which, L79 suggested the following test. Consider two states:

- 1) The parcel with the highest  $T_{vA}(k)$  is placed at  $p_A$ , and the parcel with the highest  $T_{vB}(k)$  is placed at the first pressure level below  $p_A$ .
- 2) The parcel with the highest  $T_{vB}(k)$  is placed at  $p_A$ , and the parcel with the highest  $T_{vA}(k)$  is placed at the first pressure level below  $p_A$ .

Choose the possibility that gives the lowest total enthalpy for the two parcels under consideration. We have found that this algorithm does not necessarily lead to the lowest enthalpy state; in fact, it can actually increase the total enthalpy of the system! The reason is that the

total enthalpy of the system is not considered in the test; only the total enthalpy of the two parcels is considered.

Table 6 shows the results obtained using L79's test. Parcels 37, 36, and 35 (the lowest three parcels in the given state) rise to levels 4, 5, and 7 in the reference state. The algorithm gives the impossible result that the GCAPE is  $-11.46 \text{ J kg}^{-1}$ . The corresponding correct results are given in Table 1.

We follow a slightly different approach. We compute the total enthalpy of the system for the following two states:

1) The parcel with the highest  $T_{vA}(k)$  is lifted to  $p_A$ , and the intervening parcels are shifted down by one level each.

2) The parcel with the highest  $T_{vB}(k)$  is lifted to  $p_A$ , and the intervening parcels are shifted down by one level each.

We choose the possibility that gives the lowest total enthalpy for the system. Obviously, this algorithm can never increase the total enthalpy of the system.

Once we have determined which parcel resides at the top pressure level in the reference state we *redefine*  $p_A$  to be the second pressure level from the top and repeat the test described above, considering all of the parcels whose reference-state pressures have not yet been identified. This process is continued until the reference-state pressures of all parcels have been determined.

#### REFERENCES

- Arakawa, A., and W. H. Schubert, 1974: The interaction of a cumulus cloud ensemble with the large-scale environment, Part I. *J. Atmos. Sci.*, **31**, 674-701.
- , and J.-M. Chen, 1987: Closure assumptions in the cumulus parameterization problem. *Short and Medium Range Numerical Weather Prediction*. Collection of Papers Presented at the WMO/IUGG Symposium on Numerical Weather Prediction, Tokyo, 4-8 August 1986, Special Vol., *J. Meteor. Soc. Japan.*, 107-131.
- Betts, A. K., 1982: Saturation point analysis of moist convective overturning. *J. Atmos. Sci.*, **39**, 1484-1455.
- , and M. J. Miller, 1986: A new convective adjustment scheme. Part II: Single column tests using GATE wave, BOMEX, ATEX, and arctic air-mass data sets. *Quart. J. Roy. Meteor. Soc.*, **112**, 693-709.
- Cheng, M.-D., 1989: Effects of downdrafts and mesoscale convective organization on the heat and moisture budgets of tropical cloud clusters. Part II: Effects of convective-scale downdrafts. *J. Atmos. Sci.*, **46**, 1540-1564.
- Dudhia, J., and W. M. Moncrieff, 1987: A numerical simulation of quasistationary tropical convective bands. *Quart. J. Roy. Meteor. Soc.*, **113**, 929-967.
- Krueger, S. K., 1988: Numerical simulation of tropical cumulus clouds and their interaction with the subcloud layer. *J. Atmos. Sci.*, **45**, 2221-2250.
- Lord, S. J., and A. Arakawa, 1980: Interaction of a cumulus ensemble with the large-scale environment. Part II. *J. Atmos. Sci.*, **37**, 2677-2692.
- Lorenz, E. N., 1955: Available potential energy and the maintenance of the general circulation. *Tellus*, **7**, 157-167.
- , 1978: Available energy and the maintenance of a moist circulation. *Tellus*, **30**, 15-31.
- , 1979: Numerical evaluation of moist available energy. *Tellus*, **31**, 230-235.
- Manabe, S., J. Smagorinsky, and R. F. Strickler, 1965: Simulated climatology of a general circulation model with a hydrologic cycle. *Mon. Wea. Rev.*, **93**, 769-798.
- Ooyama, K. V., 1990: A thermodynamic foundation for modeling the moist atmosphere. *J. Atmos. Sci.*, **47**, 2580-2593.
- Soong, S.-T., and W.-K. Tao, 1980: Response of deep tropical cumulus clouds to mesoscale processes. *J. Atmos. Sci.*, **37**, 2016-2034.
- Thompson, R. M., S. W. Payne, E. E. Recker, and R. J. Reed, 1979: Structure and properties of synoptic scale wave disturbances in the intertropical convergence zone of the eastern Atlantic. *J. Atmos. Sci.*, **36**, 53-72.
- Xu, K.-M., 1991: The coupling of cumulus convection with large-scale processes. Ph.D. thesis, University of California, Los Angeles, 250 pp.
- , and K. A. Emanuel, 1989: Is the tropical atmosphere conditionally unstable? *Mon. Wea. Rev.*, **117**, 1471-1479.
- Yanai, M., S. K. Esbensen, and J.-H. Chu, 1973: Determination of bulk properties of tropical cloud clusters from large-scale heat and moisture budgets. *J. Atmos. Sci.*, **30**, 611-627.

7-17-2-1993

## The Moist Available Energy of a Conditionally Unstable Atmosphere. Part II: Further Analysis of GATE Data

JUNYI WANG AND DAVID A. RANDALL

*Department of Atmospheric Science, Colorado State University, Fort Collins, Colorado*

(Manuscript received 5 April 1993, in final form 9 August 1993)

### ABSTRACT

The generalized convective available potential energy (GCAPE) observed during GATE has been analyzed using the Lagrangian algorithm of Lorenz, as modified by Randall and Wang. The effects of ice are included and are discussed in an Appendix. A high positive correlation is found between the rate of GCAPE production by large-scale processes and the observed precipitation rate, and a negative correlation between the GCAPE itself and the precipitation rate. The observed time rate of change of the GCAPE is much smaller than the rate of GCAPE production by large-scale processes.

### 1. Introduction

Lorenz (1955) defined the available potential energy (APE) as the difference between the actual total enthalpy of the atmosphere and the minimum total enthalpy that could be achieved by rearranging the mass under reversible adiabatic processes. The state of minimized enthalpy, which he called the "reference state," is also the state of maximized kinetic energy. The APE represents the portion of the nonkinetic energy that is available for conversion into kinetic energy under reversible adiabatic processes.

Recognizing that moist-adiabatic processes are, in fact, adiabatic rather than diabatic, Lorenz (1978, 1979) extended the concept of APE to the moist atmosphere, coining the term "moist available energy" (MAE). The MAE depends on both the horizontal and vertical structures of the atmosphere. As discussed by Randall and Wang (1992; hereafter referred to as Part I), the vertical "component" of the MAE (i.e., the MAE that can be detected by considering only the vertical structure of an atmospheric column) is a generalization of the convective available potential energy (CAPE), which we refer to as the generalized CAPE or GCAPE. It represents the potential energy available for convection. Unlike conventional measures of CAPE, the GCAPE includes the effects of multiple parcels originating at multiple levels, and also the effects of compensating motions in the environment. We have modified the algorithm to include the effects of ice, following the method of Ooyama (1990); see the Appendix for an explanation.

In this paper, we report a further study of the variations of the GCAPE in the GATE data. The data used are from GATE Phase III, for each of 157 observation times, which span every three hours from 0900 UTC 30 August to 2100 UTC 18 September 1974 (Thompson et al. 1979).

### 2. Method

As demonstrated in Part I, the GCAPE can be calculated by using the parcel-moving algorithm designed by Lorenz (1979). Hereafter we refer to this as the "L" algorithm, where the "L" can be interpreted as standing for either Lorenz or Lagrangian. The details of the L algorithm are described in Part I; a brief summary is as follows. A given sounding is divided into many layers, which are adiabatically and reversibly rearranged in a Lagrangian sense, that is, moved to different pressures, in such a way as to minimize the total enthalpy; see Fig. 1. Because the layers are treated as discrete units that maintain their identities in passing from the given state to the reference state, we can refer to them as "parcels." The method used to find the vertical ordering of the parcels in the reference state is a slightly modified version of the method suggested by Lorenz (1979); see Part I for an explanation. The GCAPE is determined as the difference in total enthalpy between the given state and the reference state. The L algorithm guarantees that the reference state is horizontally homogeneous, although it may have very fine vertical structure.

The L algorithm is approximate in that the continuous atmosphere is represented by a finite number of parcels; except for this discretization, the algorithm is essentially exact. Results presented in Part I, and further results to be presented in this paper, show that the

Corresponding author address: Dr. David A. Randall, Department of Atmospheric Science, Colorado State University, Fort Collins, CO 80523.

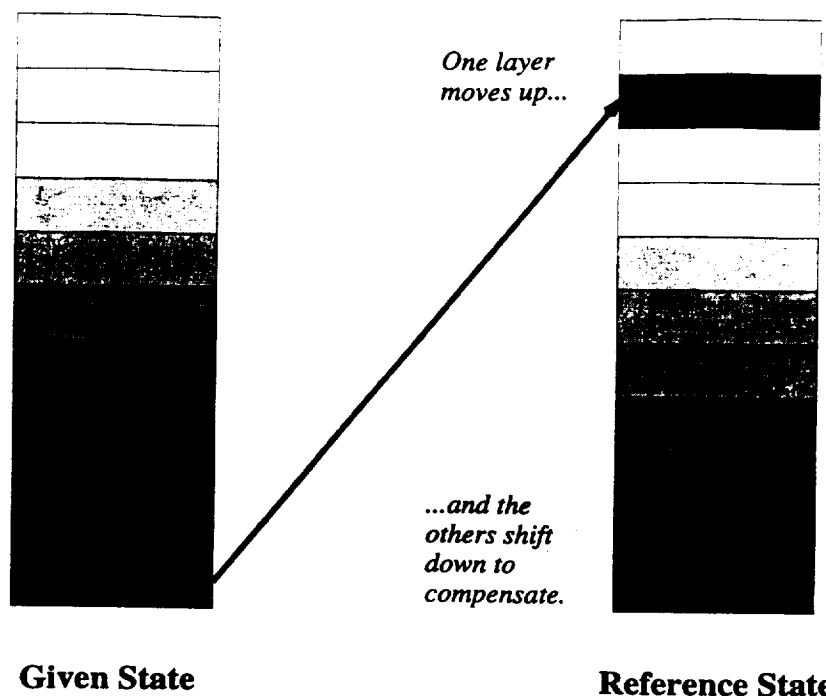


FIG. 1. Diagram illustrating the L algorithm. Layers or "parcels" of the given state are bodily reordered in the reference state.

GCAPE and reference sounding converge, that is, become independent of the number of parcels, as the number of parcels increases.

### 3. Results

First we present some results obtained with a particular GATE Phase III sounding, that for observation time 45, which is 2100 UTC 4 September 1974. This sounding was chosen because the GCAPE is particularly large (see results presented later).

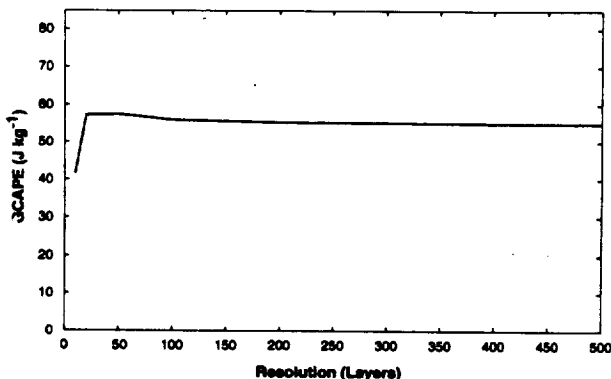


FIG. 2. The resolution dependence of the GCAPE, for GATE observation time 45. Results are plotted for up to 500 layers. The smallest number of layers considered is ten.

Figure 2 shows the resolution dependence of the GCAPE obtained with the L algorithm. Results are plotted for up to 500 layers; the smallest number of layers considered here is ten. Convergence is good with 40 layers, and excellent with 100 or more layers. The GCAPE detected is about  $55 \text{ J kg}^{-1}$ .

The dependence of the GCAPE on the vertical distributions of temperature and total mixing ratio in the given state is obviously of interest. Figure 3 shows the change of GCAPE obtained by altering the temperature or total mixing ratio, as a function of the height at which the change is made, again for GATE observation time 45. As expected, increasing the low-level temperature (or entropy) increases the GCAPE, as does decreasing the upper-level temperature (or entropy). Increasing the low-level moisture also increases the GCAPE. Increasing the moisture aloft has little effect, however.

Now we analyze the Phase III data for each observation time (every 3 hours) from 0 UTC 1 September (observation time 14) to 2100 UTC 18 September 1974 (observation time 157). We use 40 layers.

Figure 4 shows the time variation of the GCAPE. Also shown, for comparison, is the radar-observed precipitation rate. Temporal fluctuations over GATE Phase III span roughly one order of magnitude. The correlation of the GCAPE with the observed precipitation rate is  $-0.43$ . A similar result was reported by Thompson et al. (1979). The implication is that the level of convective activity, as measured by the precip-

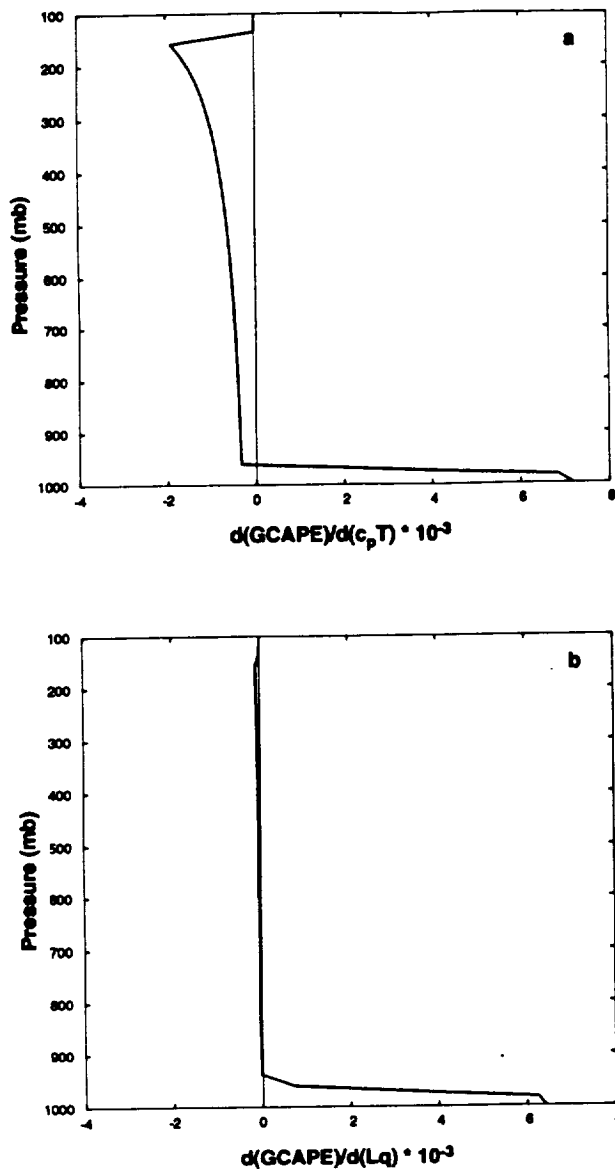


FIG. 3. The rate of change of the GCAPE with the temperature (panel a) and total mixing ratio (panel b), plotted as a function of the pressure at which the change is made, for GATE Phase III observation time 45.

itation rate, does not simply increase with the degree of convective instability; if anything, it decreases. An interpretation is that the observed degree of convective instability is strongly influenced by the rate at which convection consumes GCAPE.

We have investigated the effects of "large-scale" (i.e., nonconvective) processes on the GCAPE by the following method. First, we determine the GCAPE associated with an observed sounding. Then we consider the effects of the various nonconvective processes such as advection of temperature and moisture, adiabatic expansion, surface fluxes, and radiation. The large-scale

tendencies were obtained from the GATE analyses of Thompson et al. (1979). Radiative effects were based on the GATE radiative heating (cooling) rates calculated by Cox and Griffith (1979a,b). The surface evaporation rate and the surface sensible heat flux were obtained from Dr. E. E. Recker of the University of Washington (1992, personal communication), based on analysis of ship data by Thompson (1977). These surface fluxes were assumed to act uniformly on the air between the surface and 950 mb. For each observation time, we determined the GCAPE of a hypothetical sounding, defined as the given sounding as modified by the effects of the *nonconvective processes only*, acting over a time interval  $\Delta t$ . The difference of the GCAPEs between the hypothetical sounding and the observed sounding, divided by  $\Delta t$ , is considered to be the rate of GCAPE production by large-scale processes. We choose  $\Delta t = 3$  h, simply because the observations are available every three hours. The effects of the choice of  $\Delta t$  are discussed at the end of this section.

Figure 5a shows the time variation of the GCAPE production rate due to all nonconvective processes. Also shown, for comparison, is the radar-observed precipitation rate. There is a strong positive correlation between the rate of GCAPE production by large-scale processes and the observed precipitation rate. The correlation coefficient is 0.79. Figure 5b shows the GCAPE production rate with and without the effects of surface evaporation. The overall GCAPE production rate is greatly enhanced by the effects of surface evaporation, although its temporal fluctuations are mainly controlled by other processes.

For GATE observation time 45, Fig. 6 shows the contributions of various processes to the GCAPE production rate. The effects of large-scale vertical motion on temperature and moisture are powerful GCAPE producers, increasing the given value ( $55.79 \text{ J kg}^{-1}$ ) by about two-thirds (to  $88.94 \text{ J kg}^{-1}$ ) in three hours. Surface evaporation is of even greater importance. Radiation and the surface sensible heat flux are very minor contributors; this is consistent with the conclusions of

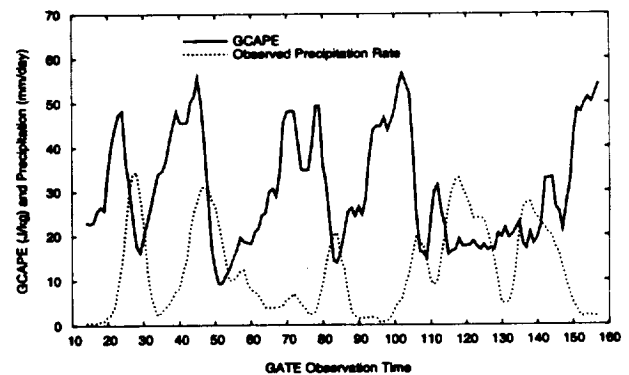


FIG. 4. The time variation of the GCAPE during GATE Phase III. Also shown, for comparison, is the radar-observed precipitation rate.

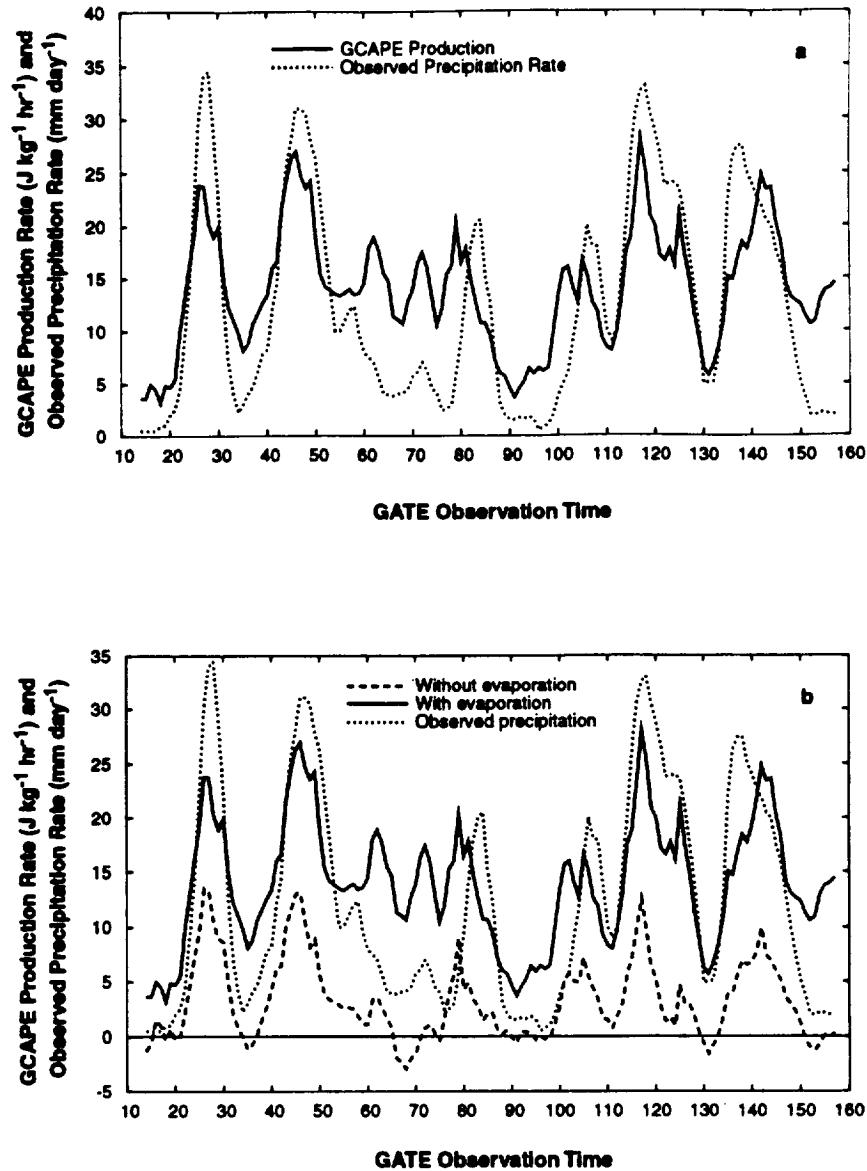


FIG. 5. (a) The time variation of the GCAPE production rate due to large-scale processes, including advection, radiation and surface fluxes, as determined. Also shown, for comparison, is the radar-observed precipitation rate. (b) The time variation of the GCAPE production rate with and without the effects of surface evaporation. The zero line is shown, for convenience. Also plotted, for comparison, is the radar-observed precipitation rate.

Lord (1982). Of course, the contributions of the various processes, as shown in Fig. 6, depend to some extent on the order in which the processes are included, but the basic conclusions given above are not sensitive to the order.

Figure 7 shows a comparison of the rate of GCAPE production by large-scale processes and the observed rate of change of the GCAPE. Each point in the figure represents one observation time. The value on the ordinate represents the observed time rate of change of

the GCAPE, while the value on abscissa represents the rate of GCAPE production by large-scale processes. It is apparent that the rate of GCAPE production by large-scale processes is generally much greater than the observed time rate of change of the GCAPE. A similar conclusion was reached by Arakawa and Schubert (1974), Lord (1982), and Xu and Arakawa (1992). The results shown in Fig. 7 imply that there is a very strong negative correlation between the time rate of change of the GCAPE due to convection and that due

*L* algorithm with 40 layers  
GATE Observation Time 45

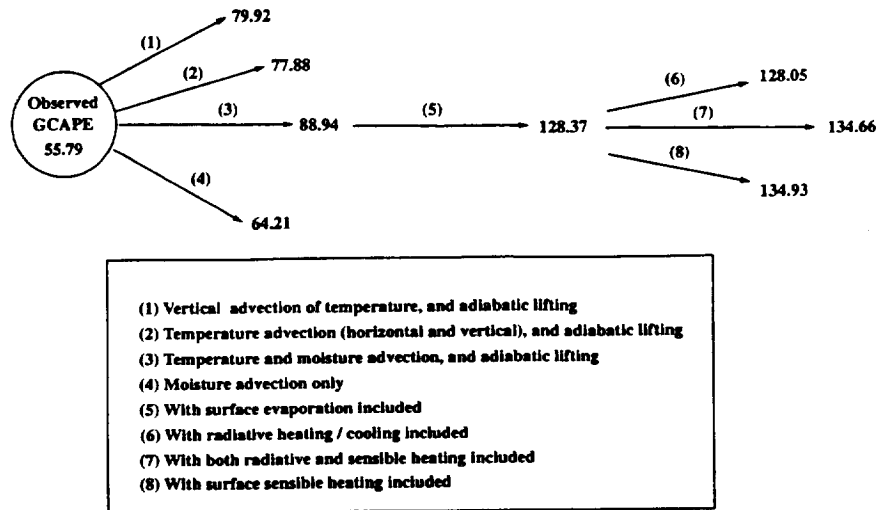


FIG. 6. For GATE Phase III observation time 45, the contributions of various processes to the GCAPE production rate. The circle represents the given state, and the numerical value inside gives the GCAPE of the given state, in  $J\ kg^{-1}$ . The arrows represent various nonconvective processes, acting over a three-hour period (see text). The numbers in parentheses next to the arrows refer to the legend in the box at the bottom of the diagram. The numbers at the ends of the arrows give the GCAPE obtained, in  $J\ kg^{-1}$ , after the action of the particular process over the specified three-hour period.

to nonconvective processes. Convection consumes GCAPE as fast as nonconvective processes can produce it. As a result, the atmosphere stays "close" to a neutral state (Arakawa and Schubert 1974), that is, the reference state. In Fig. 7, there appears to be some tendency for the strongest large-scale tendencies to be associated with negative observed time rates of change; this merits further investigation.

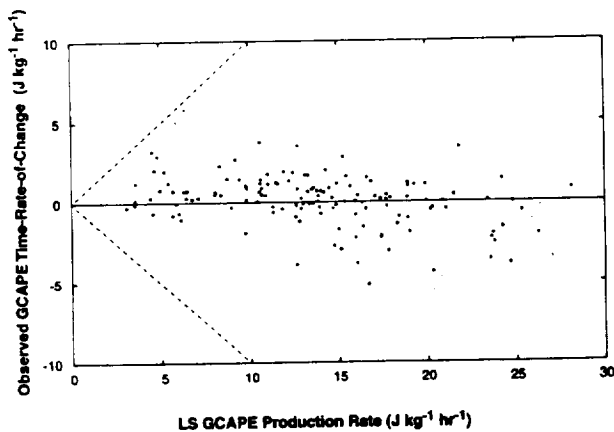


FIG. 7. A comparison of the rate of GCAPE production by large-scale processes (abscissa) and the observed rate of change of the GCAPE (ordinate). Each point represents one observation time.

As a sensitivity test, we changed  $\Delta t$  from 3 hours to 30 minutes; that is, we used the rates of change determined from the observations that are available once every 3 hours, but we applied these rates of change for

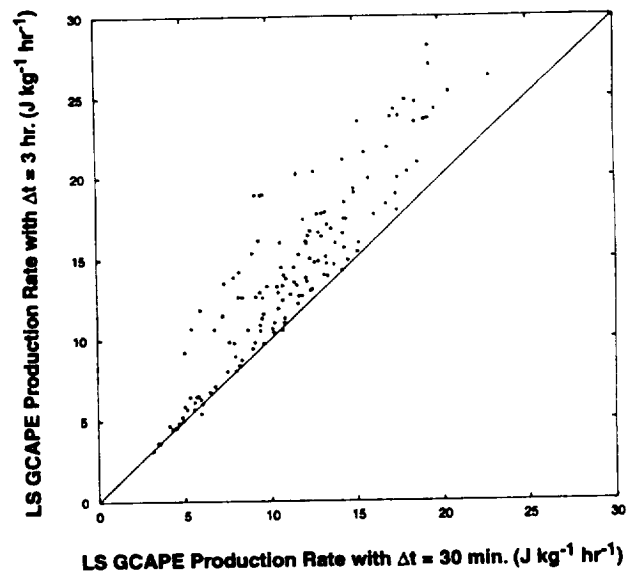


FIG. 8. A comparison of the magnitudes of the GCAPE production rates by large-scale processes with  $\Delta t = 30\ min$  and  $\Delta t = 3\ h$ .

only 30 minutes. Figure 8 shows that although the magnitudes of the GCAPE production rates by large-scale processes with  $\Delta t = 30$  minutes are generally smaller than those with  $\Delta t = 3$  h, the two estimates are nevertheless quite comparable. The positive correlations mentioned earlier, between the GCAPE production rate by the large-scale processes and the observed precipitation rate, are hardly affected. In short, our conclusions are not very sensitive to the value of  $\Delta t$ .

#### 4. Summary and conclusions

Our analysis shows that both large-scale vertical motions and surface evaporation contribute significantly to the GCAPE production rate. The observed precipitation rate is negatively correlated (temporally) with the GCAPE, but is very positively correlated with the rate of GCAPE production by large-scale processes. The observed time rate of change of the GCAPE is much smaller than the rate of GCAPE production by nonconvective processes. This implies that the convection very efficiently consumes GCAPE, converting it into convective kinetic energy, in the sense that the rate of consumption of GCAPE by the convection is almost equal to the rate of production of GCAPE by nonconvective processes.

Our results encourage us to think that a cumulus parameterization can be formulated using the concept of GCAPE and its associated reference state. The equilibrium state to which the parameterization adjusts would be the reference state used in the definition of the GCAPE. An attractive aspect of this approach is that the equilibrium state is based neither on empiricism nor on simple cloud models, but rather on the basic physics of moist available potential energy.

The L algorithm used here uses a Lagrangian approach to find the GCAPE. It seems well suited to data analysis. As discussed in Part I, an Eulerian approach offers some advantages in modeling applications. This is a subject for further research.

*Acknowledgments.* Prof. W. H. Schubert and Dr. K.-M. Xu of CSU also offered comments on this work. Prof. R. Reed, of the University of Washington, allowed us to use the GATE data as analyzed by his group. Dr. E. E. Recker of the University of Washington helped us to obtain the evaporation and precipitation data. Professor M. Yanai, UCLA, supplied the GATE radiation data, as analyzed by Cox and Griffiths (1979a,b).

Support has been provided by the National Aeronautics and Space Administration under Grant NAG5-1058 and the National Science Foundation under Grant ATM-8907414, both to Colorado State University. Computing resources were provided by the Scientific Computing Division of the National Center for Atmospheric Research, which is sponsored by the National Science Foundation.

#### APPENDIX

##### The Effects of Ice

###### a. Basic approach

For an air parcel consisting of one mass unit of dry air and  $\bar{w}$  mass units of total water, of which  $w$  units are water vapor and  $\bar{w} - w$  units are liquid water, the entropy  $s$  and enthalpy  $h$  can be expressed (Lorenz 1979) as

$$(1 + \bar{w})s = (c_p + \bar{w}c_{pw}) \ln T - R \ln(p - e) - \bar{w}R_w \ln(e) - (\bar{w} - w) \frac{L}{T} + \text{const}, \quad (\text{A.1})$$

$$(1 + \bar{w})h = (c_p + \bar{w}c_{pw})T - (\bar{w} - w)L + \text{const}, \quad (\text{A.2})$$

where  $T$  is air temperature,  $p$  is air pressure,  $e$  is water vapor pressure,  $R$  and  $R_w$  are the gas constants for dry air and water vapor,  $c_p$  and  $c_{pw}$  are the specific heat of dry air and water vapor at constant pressure, and  $L$  represents the latent heat from water vapor to liquid water. We want to consider the latent heat from water vapor to ice when the temperature is low enough.

From the Clausius-Clapeyron equation,  $L(T)$  can be written as

$$L(T) = \frac{R_w T^2}{E(T)} \frac{dE(T)}{dT}, \quad (\text{A.3})$$

where  $E(T)$  is the saturation water vapor pressure at the temperature  $T$ . Substituting (A.3) into (A.1) and (A.2), and considering the saturated case, we obtain

$$(1 + \bar{w})s = (c_p + \bar{w}c_{pw}) \ln T - R \ln[p - E(T)] - \bar{w}R_w \ln[E(T)] - (\bar{w} - w) \left[ \frac{R_w T}{E(T)} \frac{dE(T)}{dT} \right] + \text{const} \quad (\text{A.4})$$

$$(1 + \bar{w})h = (c_p + \bar{w}c_{pw})T - (\bar{w} - w) \left[ \frac{R_w T^2}{E(T)} \frac{dE(T)}{dT} \right] + \text{const}. \quad (\text{A.5})$$

By using (A.4-5), the effects of ice can be included through the saturation vapor pressure,  $E(T)$ . We follow Ooyama's (1990) method to calculate  $E(T)$ .

Ooyama (1990) pointed out that there is a discontinuity, at  $0^\circ\text{C}$ , between the specific entropy of liquid water and that of ice. By defining a freezing zone of finite width, he eliminated this discontinuity, allowing ice effects to "ramp up" smoothly rather than "switch on" discontinuously. We apply his ideas to incorporate ice effects into the GCAPE calculation, as follows.

Ooyama considered the specific entropy of condensation for an air parcel,  $C(T)$ , as a weighted combi-

nation of the specific entropy of ice,  $C_i(T)$ , and the specific entropy of liquid water,  $C_w(T)$ :

$$C(T) = \Omega_w(T)C_w(T) + \Omega_i(T)C_i(T). \quad (\text{A.6})$$

Here  $\Omega_w(T)$  and  $\Omega_i(T)$  are smooth functions:

$$\Omega_w(T) = \frac{1}{2} \left[ 1 + \tanh \left( \frac{T - T_f}{\Delta T_f} \right) \right],$$

$$\Omega_i(T) = 1 - \Omega_w(T);$$

$\Delta T_f$  is the width of the "freezing zone"; and  $T_f$  is the central temperature of the freezing zone. The expressions for  $C(T)$ ,  $C_i(T)$ , and  $C_w(T)$  are

$$C_w(T) = C_{pw} \ln \left( \frac{T}{T_0} \right) - R_w \frac{d}{dT} \left[ T \ln \left( \frac{E_w(T)}{E_{w0}} \right) \right] + \text{const}, \quad (\text{A.7})$$

$$C_i(T) = C_{pi} \ln \left( \frac{T}{T_0} \right) - R_w \frac{d}{dT} \left[ T \ln \left( \frac{E_i(T)}{E_{i0}} \right) \right] + \text{const}, \quad (\text{A.8})$$

$$C(T) = C_{pw} \ln \left( \frac{T}{T_0} \right) - R_w \frac{d}{dT} \left[ T \ln \left( \frac{E(T)}{E_{w0}} \right) \right] + \text{const}, \quad (\text{A.9})$$

where  $E_w(T)$  is the saturation water vapor pressure over a liquid water surface at temperature  $T$ , and  $E_i(T)$  is the saturation water vapor pressure over an ice surface at temperature  $T$ . Also,  $E_{w0} = 6.108$  mb is the saturation water vapor pressure over a liquid water surface at the temperature  $T_0 = 273.16$  K, and  $E_{i0} = 6.107$  mb is the saturation water vapor pressure over an ice surface at  $T_0$ .

Substituting (A.7), (A.8), and (A.9) into (A.6), we find that

$$\frac{d}{dT} \left[ T \ln \left( \frac{E(T)}{E_{w0}} \right) \right] = \Omega_w(T) \left[ T \ln \left( \frac{E_w(T)}{E_{w0}} \right) \right] + \Omega_i(T) \left[ T \ln \left( \frac{E_i(T)}{E_{i0}} \right) \right]. \quad (\text{A.10})$$

As a boundary condition, we use  $E(T_s) \rightarrow E_w(T_s)$  for  $T_s \gg T_f$ , where  $T_s = 350$  K. Integrating (A.10), we obtain

$$\left[ T \ln \left( \frac{E(T)}{E_{w0}} \right) \right] \Big|_{T_s}^T = \left[ \Omega_w(T) T \ln \left( \frac{E_w(T)}{E_{w0}} \right) + \Omega_i(T) T \ln \left( \frac{E_i(T)}{E_{i0}} \right) \right] \Big|_{T_s}^T$$

$$- \int_{T_s}^T T \ln \left[ \frac{E_w(T)}{E_{w0}} \right] d\Omega_w(T)$$

$$- \int_{T_s}^T T \ln \left[ \frac{E_i(T)}{E_{i0}} \right] d\Omega_i(T). \quad (\text{A.11})$$

We have adopted the formulas for  $E_w(T)$  and  $E_i(T)$  given in the Smithsonian meteorological tables. With (A.11), these can be used to evaluate  $E(T)$ .

In this paper, we have used  $T_f = 270.16$  K, and  $\Delta T_f = 3$  K; this corresponds to a "freezing zone" from  $-6^\circ\text{C}$  to  $0^\circ\text{C}$ . Naturally, these choices have some influence on the results that we obtain. As an example, Fig. A1 shows the GCAPE and the large-scale tendency of the GCAPE obtained with two different choices of  $\Delta T_f$ . The differences are modest.

### b. Sensitivity of the GCAPE to ice effects

The increase of the GCAPE due to ice effects, as obtained with the L algorithm, is surprisingly large: ice effects cause the GCAPE to increase from  $12.6 \text{ J kg}^{-1}$  to  $56 \text{ J kg}^{-1}$ , with 40 layers.

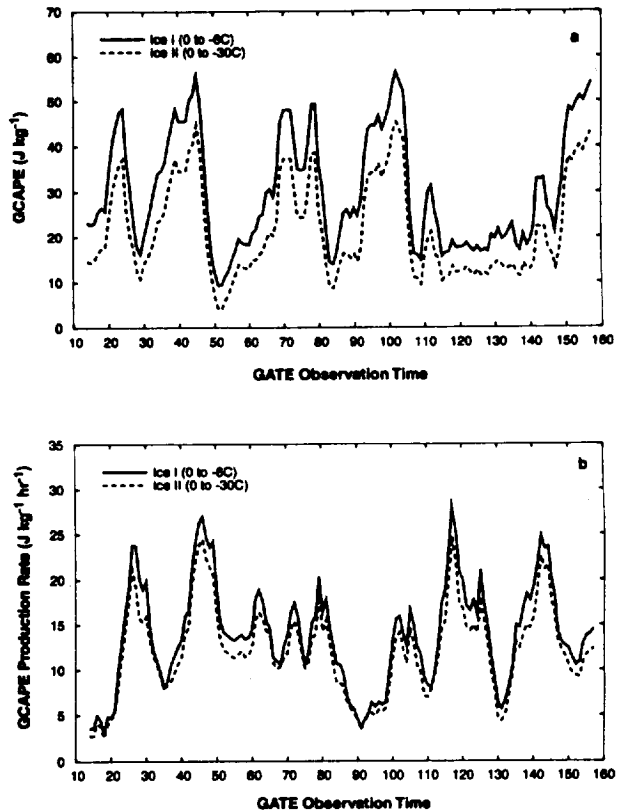


FIG. A1. Time history of the GCAPE (panel a) and the GCAPE production rate by large-scale processes (panel b), as obtained with "freezing zones" that extend from  $0^\circ\text{C}$  to  $-6^\circ\text{C}$  (solid lines) and from  $0^\circ\text{C}$  to  $-30^\circ\text{C}$  (dashed lines).

To investigate the reason for the peculiar sensitivity of the L algorithm, we use GATE observation time 45 as an example. We divide the sounding into 20 layers, numbered from the top down. By using the no-ice version of the L algorithm, we find that the reference state can be reached by moving parcel 20 of the given state to the position of parcel 2 of the given state, and shifting parcels 2 through 19 down by one level. In passing from the given state to the reference state, the enthalpy of layer 1 remains unchanged, the enthalpy of layer 2 is reduced, and the enthalpies of layers 3 to 20 are increased. The total enthalpy increase of layers 3 to 20 is less than the enthalpy decrease of layer 2; that is, the system's total enthalpy decreases, by  $10 \text{ J kg}^{-1}$ .

Referring to (A.2), we see that the enthalpy per unit mass thus consists of a temperature component [the first term on the rhs of (A.2)] and a liquid/ice component (the second term). For the lifted parcel, the change due to condensate is negative, while the change due to warming is actually positive. For the subsiding parcels, the change due to warming is positive, while the change in the liquid/ice component is zero. For the entire column, warming increases the enthalpy by  $2270.1 \text{ J kg}^{-1}$ , while condensation decreases the enthalpy by  $2280.1 \text{ J kg}^{-1}$ . The net decrease in the enthalpy,  $10 \text{ J kg}^{-1}$ , is the small difference between these large numbers.

Now suppose that ice effects are included. Not surprisingly, it turns out that the parcels are rearranged in the same way as before. The GCAPE is  $57.2 \text{ J kg}^{-1}$  this time, however! Obviously, ice formation influences only the enthalpy of the upward-moving parcel; it has no effect on the enthalpy of the subsiding, ice-free parcels. The temperature of the lifted parcel increases, but its condensate mixing ratio also increases; according to (A.2), the warming increases the enthalpy, but the additional condensate decreases the enthalpy. The additional warming due to ice is  $2.25 \text{ K}$ . On the other hand, the additional condensate formed

amounts to  $1.3 \times 10^{-2} \text{ g kg}^{-1}$ . For the whole column, warming increases the enthalpy by  $2384.6 \text{ J kg}^{-1}$ , while the formation of liquid and ice decreases it by  $2441.8 \text{ J kg}^{-1}$ . The net effect of ice, therefore, is to decrease the enthalpy by  $47.2 \text{ J kg}^{-1}$ , implying an increase of the GCAPE by the same amount. This is an enormous increase from the  $10 \text{ J kg}^{-1}$  obtained without ice, but is not much compared to the individual "warming" and "condensate" terms that nearly cancel.

#### REFERENCES

- Arakawa, A., and W. H. Schubert, 1974: The interaction of a cumulus cloud ensemble with large-scale environment, Part I. *J. Atmos. Sci.*, **31**, 674–701.
- Cox, S. K., and K. T. Griffith, 1979a: Estimates of radiative divergence during Phase III of the GARP Atlantic Tropical Experiment. Part I: Methodology. *J. Atmos. Sci.*, **36**, 576–585.
- , and —, 1979b: Estimates of radiative divergence during Phase III of the GARP Atlantic Tropical Experiment. Part II: Analysis of Phase III Results. *J. Atmos. Sci.*, **36**, 586–601.
- Lord, S. J., 1982: Interaction of a cumulus cloud ensemble with the large-scale environment. Part III: Semi-prognostic test of the Arakawa-Schubert cumulus parameterization. *J. Atmos. Sci.*, **39**, 88–103.
- Lorenz, E. N., 1955: Available potential energy and the maintenance of the general circulation. *Tellus*, **7**, 157–167.
- , 1978: Available energy and the maintenance of a moist circulation. *Tellus*, **30**, 15–31.
- , 1979: Numerical evaluation of moist available energy. *Tellus*, **31**, 230–235.
- Ooyama, K. V., 1990: A thermodynamic foundation for modeling the moist atmosphere. *J. Atmos. Sci.*, **47**, 2580–2593.
- Randall, D. A., and J. Wang, 1992: The moist available energy of a conditionally unstable atmosphere. *J. Atmos. Sci.*, **49**, 240–255.
- Thompson, R. M., Jr., 1977: Preliminary heat and moisture budgets over the B-scale ship array during Phase III of GATE. M.S. thesis, University of Washington, 103 pp.
- , S. W. Payne, E. E. Recker, and R. J. Reed, 1979: Structure and properties of synoptic scale wave disturbances in the intertropical convergence zone of the eastern Atlantic. *J. Atmos. Sci.*, **36**, 53–72.
- Xu, K.-M., and A. Arakawa, 1992: Semiprognostic tests of the Arakawa-Schubert cumulus parameterization using simulated data. *J. Atmos. Sci.*, **49**, 2421–2436.

115

**DISSERTATION**

**GENERALIZED CONVECTIVE AVAILABLE POTENTIAL ENERGY AND  
ITS APPLICATION TO CUMULUS PARAMETERIZATION**

**Submitted by**

**Junyi Wang**

**Department of Atmospheric Science**

**In partial fulfillment of the requirements**

**for the Degree of Doctor of Philosophy**

**Colorado State University**

**Fort Collins, Colorado**

**Spring 1994**



ABSTRACT OF DISSERTATION  
GENERALIZED CONVECTIVE AVAILABLE POTENTIAL ENERGY AND  
ITS APPLICATION TO CUMULUS PARAMETERIZATION

Based on the concept of Moist Available Energy (MAE) of Lorenz (1978, 1979), the Generalized Convective Available Potential Energy (GCAPE) was defined as the vertical component of the MAE and a measure of the conditional instability of a column atmosphere. The GCAPE represents the potential energy available for convection. Unlike conventional measures of convective available potential energy (CAPE), the GCAPE includes the effects of multiple parcels originating at multiple levels, and also the effects of compensating motions in the environment. The modified Lorenz Parcel-Moving Algorithm for calculating GCAPE was presented. Ice effects were included, based on the approach of Ooyama (1990). The GCAPE of Global Atmosphere Research Program's Atlantic Tropical Experiment (GATE) Phase III data was analyzed.

The Lorenz algorithm is a Lagrangian algorithm. To be better suited for modeling and other application, an Eulerian "penetrator" algorithm is proposed. The results from the penetrator algorithm are discussed.

As one of its applications, the GCAPE has been used in a cumulus parameterization. By using Nitta's (1975) model, the cloud-base mass flux for each cloud type can be calculated diagnostically. Through a key assumption in which the GCAPE and its related reference state are used, we can use Nitta's model to calculate the cloud-base mass flux in a prognostic way. With the cloud-base mass flux known, the Arakawa-Schubert (1974) model can be used to obtain the cloud properties and the feedbacks of convection on the



large-scale fields. The effects of downdrafts were included by following Johnson's (1976) scheme. We related the adjustment time scale to the GCAPE production rate of large-scale processes. The proposed cumulus parameterization has been tested with GATE Phase III data. The calculated precipitation rate, warming and drying of the large-scale fields by convection are generally similar to those observed. Problems of the proposed cumulus parameterization are also discussed. Including the anvil cloud effects in a more detailed way is a key remaining problem.

Junyi Wang  
Department of Atmospheric Science  
Colorado State University  
Fort Collins, CO 80523  
Spring, 1994

